

Cancer Brachytherapy at the Nanoscale: An Emerging Paradigm

Sanchita Ghosh, Sophia J. Lee, Jessica C. Hsu, Sudipta Chakraborty, Rubel Chakravarty,* and Weibo Cai*



Cite This: *Chem. Biomed. Imaging* 2024, 2, 4–26



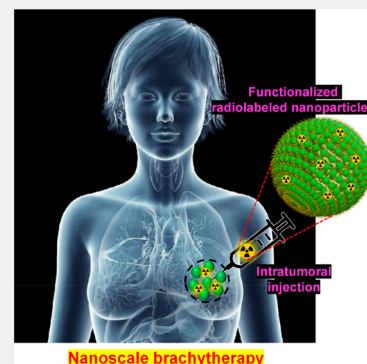
Read Online

ACCESS |

Metrics & More

Article Recommendations

ABSTRACT: Brachytherapy is an established treatment modality that has been globally utilized for the therapy of malignant solid tumors. However, classic therapeutic sealed sources used in brachytherapy must be surgically implanted directly into the tumor site and removed after the requisite period of treatment. In order to avoid the trauma involved in the surgical procedures and prevent undesirable radioactive distribution at the cancerous site, well-dispersed radiolabeled nanomaterials are now being explored for brachytherapy applications. This emerging field has been coined “nanoscale brachytherapy”. Despite present-day advancements, an ongoing challenge is obtaining an advanced, functional nanomaterial that concurrently incorporates features of high radiolabeling yield, short labeling time, good radiolabeling stability, and long tumor retention time without leakage of radioactivity to the nontargeted organs. Further, attachment of suitable targeting ligands to the nanoplateforms would widen the nanoscale brachytherapy approach to tumors expressing various phenotypes. Molecular imaging using radiolabeled nanoplateforms enables noninvasive visualization of cellular functions and biological processes *in vivo*. *In vivo* imaging also aids in visualizing the localization and retention of the radiolabeled nanoplateforms at the tumor site for the requisite time period to render safe and effective therapy. Herein, we review the advancements over the last several years in the synthesis and use of functionalized radiolabeled nanoplateforms as a noninvasive substitute to standard brachytherapy sources. The limitations of present-day brachytherapy sealed sources are analyzed, while highlighting the advantages of using radiolabeled nanoparticles (NPs) for this purpose. The recent progress in the development of different radiolabeling methods, delivery techniques and nanoparticle internalization mechanisms are discussed. The preclinical studies performed to date are summarized with an emphasis on the current challenges toward the future translation of nanoscale brachytherapy in routine clinical practices.



KEYWORDS: Brachytherapy, cancer, intratumoral injection, minimally invasive, nanomaterials, PET, radiolabeling, radiation therapy, SPECT, theranostics

INTRODUCTION

Cancer is a major cause of human mortality by non-communicable diseases worldwide. According to GLOBOCAN 2020 estimation, almost 10 million people died from cancer in the year 2020 alone.¹ Along with surgery, chemotherapy and immunotherapy, radiotherapy or radiation therapy (RT) is one of the most effective therapeutic procedures for treating locoregional solid cancers.^{2,3} Currently, two-thirds of cancer patients are treated by RT in conjunction with other modalities of therapy (e.g., surgery, chemotherapy). RT uses ionizing radiation to kill cancer cells or slow down the growth of cancerous cells by damaging DNA. The three main categories of RT include external beam RT (EBRT), internal RT or brachytherapy, and systemic RT. In EBRT, high-energy electron or proton beams generated from a linear accelerator are used to deliver radiation doses to the targeted area while keeping the radiation source outside of the patient's body.⁴ In systemic RT, generally cold carrier molecules which may have targeting moieties (i.e., monoclonal antibody, protein, peptide, etc.) are labeled with suitable radionuclides, the formulation

known as radiopharmaceuticals.⁵ Also, in some cases, the radiopharmaceutical is a simple salt such as $[^{64}\text{Cu}]\text{CuCl}_2$ which can directly be administered.^{6–8} The radiopharmaceuticals are generally administered by means of intravenous injection or through oral route to provide the requisite radiation doses to the cancerous site. In internal RT or brachytherapy, sealed radioactive sources are implanted in or near the tumor.⁹ In this therapeutic modality, radioactive seeds are implanted within the body using catheters associated with intracavitary, interstitial or intraluminal applicators. These radioactive sources are either implanted permanently or removed safely after the treatment is over. Brachytherapy

Received: September 1, 2023

Revised: October 9, 2023

Accepted: November 1, 2023

Published: November 21, 2023



seeds are capable of providing high doses of radiation precisely to the target volume with minimal radiation exposure to healthy tissues. Additionally, short treatment time and cost effectiveness make brachytherapy an efficient modality for treatment of solid tumors.

From a clinical perspective, brachytherapy is a promising choice for the treatment of breast, prostate, cervix, eye, head, and neck carcinoma as a monotherapy or associated with surgery.^{9–14} However, a substantial cause for concern involves the operational and logistical complexities related to brachytherapy seed implantation. As reported by the American Brachytherapy Society, the invasive radioactive seed implantation procedure often caused acute bleeding, infection, and cardio pulmonary disease when cancer patients with other comorbidities were subjected to brachytherapy.¹⁵ In this procedure, the radioactive seeds might get displaced from the site of administration and give radiation doses to the undesired organs or tissues. Furthermore, trained professionals with accurate seed implantation and mapping technology are required for the successful treatment of malignancy using brachytherapy. Moreover, there are reports that the breast cancer patients treated with conventional brachytherapy suffered from infections, skin ulcers, and fractured ribs.¹⁶

Due to the rapid growth of nanoscience and nanotechnology, it can be an appealing option to overcome the shortcomings related to conventional brachytherapy.¹⁷ Recently, several preclinical studies reported preparation of injectable nanometer-sized brachytherapy seeds to circumvent the limitation of conventional brachytherapy.^{18–23} This new technique is known as “nanoscale brachytherapy” or “nano-brachytherapy” (Figure 1). In nanoscale brachytherapy,

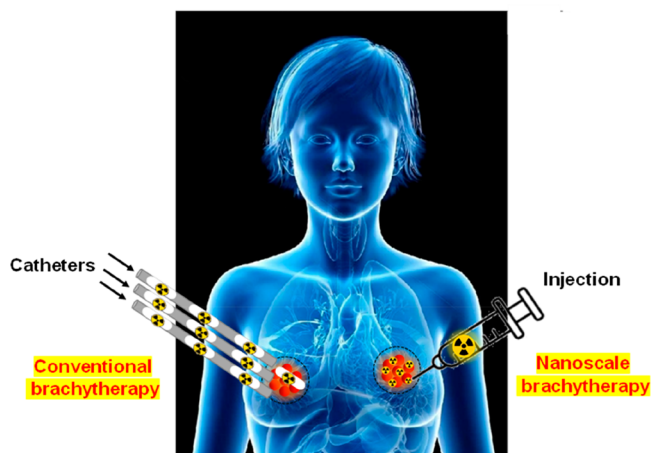


Figure 1. A schematic representation showing catheters based conventional brachytherapy, an invasive procedure, and injectable brachytherapy, a minimally invasive procedure.

colloidal solutions of radioactive NPs are injected intratumorally using smaller needles instead of seed implantation, which significantly reduces the invasiveness and trauma caused by conventional strategies.²¹ Most importantly, seed removal is not required, and this therapeutic procedure can be performed in an unshielded room, which is not possible in the standard protocol for brachytherapy. Additionally, it is also possible to formulate patient specific doses. Above all, very small tumors can be treated with nanoscale brachytherapy techniques. Lastly, the nanoscale brachytherapy agents made of high Z nanomaterials are capable to deliver radioisotopes for

molecular imaging as well as RT.²⁴ By self-sensitization, these high Z nanomaterials enhance radiation effects which may reduce radioactivity requirements as compared to conventional brachytherapy.²⁵

The distribution of nanoscale brachytherapy agents in the clinically relevant tissues must be measured noninvasively in order to confirm uptake and retention at the tumor site with minimal uptake in nontarget tissues. For noninvasive and repetitive imaging of nanoscale brachytherapy agents at the tumor site and monitoring the therapeutic efficacy in cancer patients, molecular imaging tools are attracting increasing attention of researchers and clinicians. Traditionally, imaging modalities have been categorized into two groups (Figure 2). The first group generally includes medical imaging modalities such as ultrasound imaging, computed tomography (CT) and magnetic resonance imaging (MRI), which provide anatomical information. The other group includes single photon emission computed tomography (SPECT), positron emission tomography (PET) and optical imaging, which can provide information regarding cellular functions and corresponding molecular processes. However, the latest developments in contrast agents and imaging technologies have now allowed MRI and CT also to be used as molecular imaging modalities. The characteristics of different imaging modalities are summarized in Table 1. Since, nanoscale brachytherapy agents use radioisotopes as the label, SPECT or PET imaging offers the obvious choice for visualization of their *in vivo* distribution. Nevertheless, the other imaging modalities such as CT, MRI or optical imaging can also be applied based on the intrinsic characteristics of the nanomaterials. The different imaging modalities have their inherent limitations, such as, poor sensitivity (for CT and MRI), low spatial resolution (for SPECT and PET) and limited penetration depth (for optical imaging). The nanoscale brachytherapy agents can offer the scope of exploring the synergistic benefits of two or more imaging modalities in combination, thereby, outweighing their individual limitations.

In this Review, we discuss the recent advances in nanoscale brachytherapy to date. The different radiolabeling methods are described, and their pros and cons are highlighted. Preclinical studies in this field are summarized and the possibilities of translation to clinic are discussed.

■ RADIOLABELING METHODS

The method adopted for radiolabeling is an important factor when constructing stable radiolabeled formulations. Ideally, the process should be facile, robust, safe, and highly efficient.^{31,32} Another factor to consider is the radiolabeling modification that should be performed in such a way that the physicochemical properties and the pharmacokinetics of NPs are not altered by the influence of high reaction temperature, reaction time, and purification procedures. Radiochemical yield (RCY), radiochemical stability (RCS), and radiochemical purity (RCP) are the three key aspects of any kind of radiolabeling method. RCY is “the amount of activity in the product expressed as the percentage (%) of related starting activity utilized in the considered process (e.g., synthesis, separation, etc.).”³³ Thus, achieving a high RCY for any kind of therapeutic application is desirable. RCS is the measurement of the strength of bonding between NPs and the radioisotope after radiolabeling. It provides information about the leakage of radioisotope from the radiolabeled agents to prevent the misinterpretation of results or unwanted doses to healthy

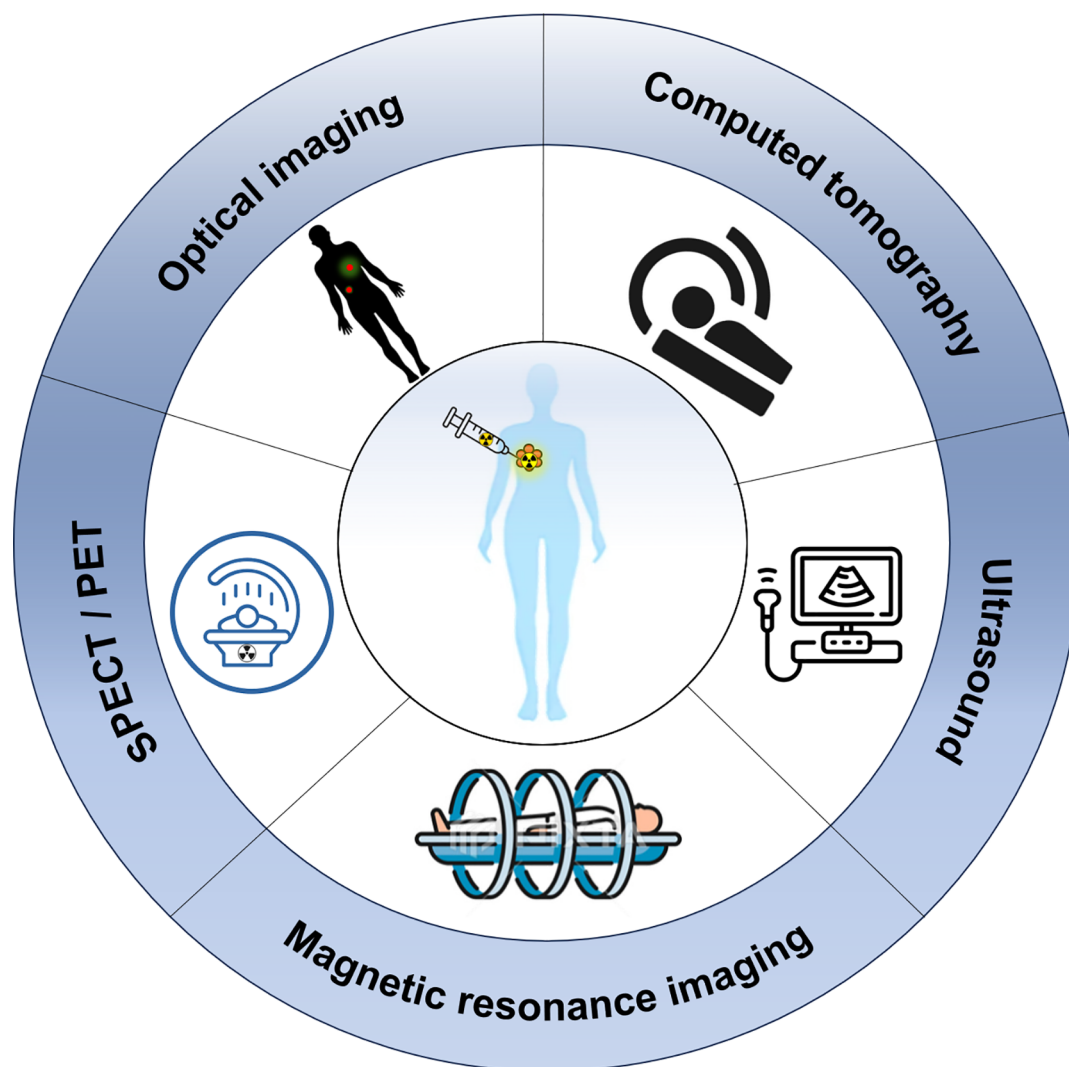


Figure 2. Different imaging modalities that can be used in nanoscale brachytherapy.

Table 1. Characteristics of Different Imaging Modalities

Imaging modality	Sensitivity	Spatial resolution	Penetration depth	Imaging probe	Reference
SPECT/PET	pM	~a few mm	no limit	radioisotopes such as, ^{18}F , ^{177}Lu , ^{198}Au , etc.	26
MRI	mM– μM	~100 μm	no limit	magnetic nanomaterials	27
CT	>mM	~100 μm	no limit	nanomaterials containing high Z elements (Au, Re, Yb, etc.)	28
Optical imaging	nM–pM	~a few mm (<i>in vivo</i>), sub $\sim\mu\text{m}$ (<i>in vitro</i>)	several cm	fluorescent dyes, quantum dots, up-conversion nanoparticles	29
Ultrasound	~mM	~a few mm	3–30 cm	functional nanoparticles (inorganic or organic) incorporated to ultrasound contrast agents such as microbubbles	30

organs on *in vivo* administration. It is generally measured in phosphate buffered saline (PBS) or human serum medium at 37 °C. RCP is the amount of radioactivity present in the sample in the desired form of radiolabeled species. Hence, the pertinent radiolabeling method must exhibit radiolabeled NPs with high RCS and RCP. Radiolabeling methods have been broadly classified into four different types: A) chelator-based radiolabeling; B) bombardment of presynthesized NPs with hadronic projectiles; C) synthesis of NPs using hot (radioactive) and cold (nonradioactive) precursors; D) chelator-free radiolabeling. These radiolabeling methods have been illustrated schematically in Figure 3. In general, the radio-

labeling method should be judiciously chosen depending on the type of radioisotope and practicability while taking into consideration “ALARA” (as low as reasonably achievable) guidelines. Below, we briefly discuss each radiolabeling method with its merits and demerits.

Chelator-Based Radiolabeling

Traditionally, in the chelator-based radiolabeling method, a coordination or covalent bond is formed between the radioisotopes and the chelators. Generally, nonmetallic radioisotopes (i.e., ^{18}F , ^{11}C , ^{131}I) can bind with NPs by covalent bond formation.^{34–36} However, the bond formation between metallic radioisotopes (e.g., ^{64}Cu , $^{99\text{m}}\text{Tc}$, ^{89}Zr) and the NPs

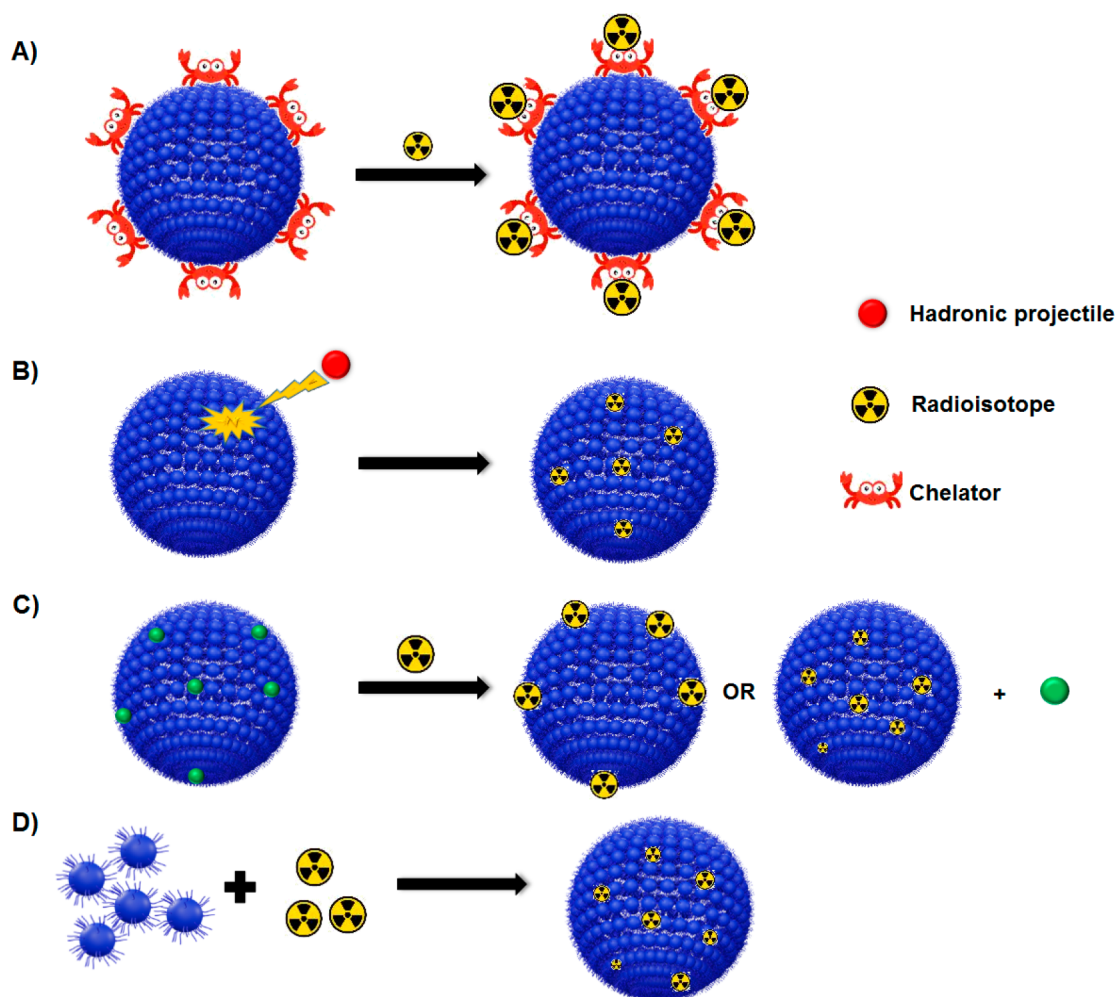


Figure 3. Schematic diagram of different radiolabeling strategies. A) Chelator-based radiolabeling, B) Radiolabeling by bombarding hadronic projectile, C) Chelator-free radiolabeling, D) Generating nanomaterials from radioactive precursors.

can only be achieved by forming coordination bond with the chelators. Therefore, coordination chemistry plays a crucial role in effective binding of radionuclides to the desired NPs.^{36,37}

The chelators are used to bind the radioisotope with two or more coordination bonds to form stable metal complexes leading to high RCS.³⁸ If the RCS is poor, a misleading signal can be produced while imaging or the radioisotope can give undesired doses to the healthy organs and tissues. Due to this reason, the choice of chelators for each kind of radioisotope is an essential factor.^{39–41} In this scenario, coordination chemistry plays a key role in understanding the coordination number, geometry, ionic radii, and charge of the radioisotope for the successful synthesis of radiopharmaceuticals. The assessment of radiometal hardness is crucial in selecting the appropriate ligand containing hard/soft donor atoms. This aids in enhancing the kinetic inertness of the coordination complex. In the context of improving thermodynamic stability, polydentate ligands offer higher stability by the chelating effect and, thus, are the better choice in comparison to the monodentate ligands. Polydentate ligands are categorized into two types: acyclic or linear chelators and macrocyclic chelators.⁴² Although acyclic or linear chelators can readily form complex, macrocyclic chelators have higher complexation stability, due to their rigid, predefined structures. However,

chelation with macrocyclic ligands suffers from slow kinetics and may require high temperatures and prolonged reaction time which can damage biologically relevant NPs such as polymers, liposomes, dendrimers, etc. Therefore, chelation between macrocyclic chelators and heat-sensitive NPs is often done post complexation.⁴³ Based on the aforesaid discussion, any ideal chelator should be able to form a highly stable complex under moderate conditions (neutral pH, room temperature) while attaining requisite thermodynamic stability and kinetic inertness under *in vivo* conditions.^{39–41}

Bifunctional chelators are extensively studied for the radiolabeling of NPs.⁴⁴ A bifunctional chelator consists of a reactive functional group containing a chelating ligand which binds to the NP surface and a chelating unit which binds to the radionuclide. The conjugation of bifunctional chelators is based on the bond formation with the functional groups present on the surface of NPs. For instance, amine conjugation is possible with the chelators containing NHS ester, anhydride or isothiocyanate group, whereas carboxylic acid conjugation is done by via carbodiimide couplings and thiol can be conjugated via maleimide coupling. The major drawback of this process is that the metal complex can be dissociated within the biological system due to enzymatic action. A few examples of chelators are dodecane tetra acetic acid-based chelators (DOTA) (used for ⁶⁸Ga, ¹¹¹In, ¹⁸⁸Re labeling), 1,4,7-

triazacyclononane- N,N',N'' -triacetic acid-based chelators (NOTA) (used for $^{67}\text{Ga}/^{68}\text{Ga}$ and ^{64}Cu labeling), diethylenetriaminepentaacetic acid based chelators (DTPA) (used for $^{99\text{m}}\text{Tc}$, ^{111}In , and ^{68}Ga labeling), etc.⁴⁵ Another approach in chelator-based radiolabeling is the ionophore-based method, wherein an ionophore ligand forms an ionophore complex with a radiometal. This complex can cross the lipid membrane, subsequently releasing the radiometal inside the vesicles for transchelation.⁴⁶ This method is utilized for vesicle-based NPs such as liposomes and exosomes. In comparison to surface labeling of NPs, this strategy is more advantageous as high RCS is achieved. Examples of common ionophores include oxine (^{111}In , ^{225}Ac , ^{177}Lu labeling), acetylacetonone (^{111}In labeling), A23187 (^{111}In , ^{90}Y labeling) etc.⁴⁶ The primary concern of chelator-based radiolabeling is 2-fold: the potential leaching of radiometals from the complex by dissociation *in vivo* and the potential alteration of the physicochemical properties of NPs following chelation.

Radiolabeling by the Bombardment of NPs with Hadronic Projectiles

This methodology involves the bombardment of NPs with hadronic projectiles such as neutrons and protons. Following bombardment, several of the NP atoms undergo a nuclear reaction, inducing direct radiolabeling of those atoms. This method is dependent on bombardment time, energy, and current of the particle beam. For instance, when a 16 MeV proton beam was applied to ^{18}O enriched alumina NPs, it converted ^{18}O into ^{18}F via $^{18}\text{O}(\text{p}, \text{n})^{18}\text{F}$ reaction without modifying the crystal structure.⁴⁷ A similar approach was taken for radiolabeling Al_2O_3 NPs with ^{13}N via $^{16}\text{O}(\text{p}, \alpha)^{13}\text{N}$ nuclear reaction.⁴⁸ Alternatively to the proton activated radiolabeling process, neutron activation was also utilized for radiolabeling holmium-based NPs via $^{165}\text{Ho}(\text{n}, \gamma)^{166}\text{Ho}$ reaction in a nuclear reactor.⁴⁹ Due to the insertion of the radioisotope into the lattice of NPs, this strategy provides a possibility of high RCY values. A novel approach to achieving an advantageous, high RCS includes the control of radiolabeling location. In this method, boron nitride nanotubes (BNNTs) were radiolabeled with ^{153}Sm via $^{152}\text{Sm}(\text{n}, \gamma)^{153}\text{Sm}$ and ^{159}Gd via $^{158}\text{Gd}(\text{n}, \gamma)^{159}\text{Gd}$ nuclear reactions.⁵⁰ However, the NP structure and the properties of biomolecules conjugated on the surface of the NPs can be altered upon exposure to a high-energy proton or neutron beam. This method also requires a proton or neutron beam source which involves complex instrumentation facilities that are not readily available everywhere, limiting the application.

Chelator-Free Radiolabeling

Radiolabeling of NPs in absence of a chelator is an emerging concept in the field of nuclear medicine.^{51–53} In this strategy, a radionuclide is directly incorporated into the core, or on the surface, of the NPs without any external chelating agent. Thus, this method is straightforward and time efficient in comparison to chelator-based radiolabeling methods. The absence of chelators not only decreases the reaction steps but also conserves the integrity of NPs as the bulky chelator molecule can affect biodistribution. The chelator-free radiolabeling is done either by adsorption or radioisotope exchange. Chemisorption occurs when two oppositely charged moieties approach each other, forming a chemical bond due to the higher binding affinity between the radioisotope and the NPs. Similarly, in physisorption, charged radioisotopes interact with the NPs either by van der Waals interaction or weak

electrostatic interactions, without compromising the physicochemical properties of the NPs. This method is especially important when coordination bond formation is not possible for the radioisotope. For example, inserting $^{75}\text{As}^{\text{III}}$ and $^{75}\text{As}^{\text{V}}$ ($^* = 71, 72, 74, 76$) in the crystal of NPs through a coordination bond formation is difficult.⁵⁴ However, it is possible to trap ^{75}As by forming a complex with iron oxide NPs that have an 84.2% labeling yield within 2 h. Unfortunately, chemical adsorption may require high temperatures, potentially altering the properties of heat-sensitive NPs. Moreover, the interaction between radionuclide and the NP must possess sufficient strength to bypass RCS issues that have been reported for ^{18}F labeled $\text{Fe}_3\text{O}_4@(\text{OH})_3$ NPs.⁵⁵ The exploration of the physisorption process has been limited due to the low RCS resulting from weak interactions between the radioisotopes and the NPs.

Radioisotope exchange is another chelator-free radiolabeling method containing two classes: heterogeneous (exchange happens between different atoms) and homogeneous (exchange happens between same atoms). For example, ^{19}F and ^{18}F have been exchanged for the radiolabeling of up-converting NPs (UCNPs).⁵⁶ Although the major purpose of this method is simplicity, very few reports attesting to this method's success have been documented.

Using "Hot" and "Cold" Precursors

In this radiolabeling strategy, a mixture of radioactive (termed as "hot") and nonradioactive (termed as "cold") precursors are taken together in order to prepare intrinsically radiolabeled NPs in a single step.^{57–61} Along with its straightforward nature, this strategy offers a quick protocol rendering it a widely used nonchelator based radiolabeling method. This method is based upon radiochemical doping as trace level of radioactive precursor (ranging from picomolar to nanomolar concentration) is added in the nonradioactive precursor leading to coprecipitation, while simultaneously incorporating radioisotope in the crystal lattice of NPs. The enhanced radiochemical stability of the radioisotope component in the crystal lattice preserves the inherent pharmacokinetics of NPs. In order to obtain high RCY, the solubility of both hot and cold precursor should be high. Most of the radionuclides are delivered in aqueous medium. As such, this radiolabeling procedure can only be conducted in an aqueous medium. Additionally, the ionic charge and ionic radius of the radionuclide should be comparable with the nonradioactive ion. Generally, radiometal ions are capable of being incorporated in the nonradioactive crystal lattice. For instance, different kind of gold NPs have been labeled with ^{199}Au , ^{198}Au and iron oxide NPs with ^{59}Fe .^{62–64}

■ RADIONUCLIDES FOR NANOSCALE BRACHYTHERAPY

Different radionuclides are chosen for nanoscale brachytherapy based on decay characteristics and the potential radiolabeling of NPs. These radionuclides emit alpha particles, beta particles, and Auger electrons, which emit radiation causing damage to the tissues. For maximum therapeutic efficacy, the radionuclides which emit particles having high linear energy transfer (LET) are preferred. Additionally, the following parameters must be evaluated before choosing the radionuclides:

- i) Physical and biological half-life
- ii) Energy of the different emitted particles and their penetration depth in tissues

- iii) Daughter products
- iv) Purity of the radionuclide
- v) Size of the tumor
- vi) Uptake and retention of radiolabeled NPs within tumor volume
- vii) Stability of the radiolabeled NPs under *in vivo* conditions and their toxicity.

In this section, we briefly summarize the radiation effects caused by emission of alpha particles, beta particles, and Auger electrons.

Alpha (α) Particle Emitter

An α particle is made of a helium (^4He) nucleus with a +2-charge emitted by radionuclides while undergoing radioactive decay. Alpha particles have the highest LET which is nearly 80 keV/ μm . Hence, they can deposit their whole energy within a cell diameter of 50–100 μm .⁶⁵ The biological effectiveness and cytotoxic effect of alpha particles are 500 times greater than those of beta particles. Primarily, alpha particles break the double strand of DNA within the cell nucleus, leading to delaying the G2 phase and chromosomal damage.⁶⁶ Thus, alpha therapy is suitable for treating small or microscopic sized tumors. Although more than 100 alpha emitting radionuclides are available, the majority of them have inappropriate half-lives for therapeutic use and/or noneconomical production routes. Some may exhibit unsuitable chemical properties that restrict their applicability in nuclear medicine.^{67,68} Presently, radium-223,224 ($^{223,224}\text{Ra}$), thorium-226,227 ($^{227,226}\text{Th}$), actinium-225 (^{225}Ac), astatine-211 (^{211}At), bismuth-212, 213 ($^{212,213}\text{Bi}$) are the α -emitters are used for therapy. Table 2 summarizes the

Table 2. Physical Characteristics of α -Emitting Radioisotopes

Radionuclide	Half-life	Mode of decay	Energy (keV)	Principal γ -component E in keV (% abundance)
^{211}At	7.2 h	α, γ	5982.4	687.0 (0.3)
^{223}Ra	11.4 d	α, γ	5979.3	269.4 (13.6)
^{224}Ra	3.6 d	α, γ	1900.0	241.0 (3.9)
^{225}Ac	10.0 d	α, γ	5935.1	99.7 (3.5)
^{212}Bi	60.6 min	α, γ	6207.1	727.2 (11.8)
^{213}Bi	45.6 min	α, γ	5982.0	439.7 (27.3)
^{226}Th	30.9 min	α, γ	4980.0	111.1 (3.29)
^{227}Th	18.7 d	α, γ	5900.0	236.0 (11.2)

nuclear properties of these α -emitters. Among the aforementioned radionuclides, short half-lives of ^{213}Bi , ^{212}Bi and ^{226}Th limit their applicability in the field of radiation therapy.

For clinical studies with ^{227}Th , it is imperative to develop enhanced purification and isolation procedures. The primary contributing factor behind the limited application of $^{223,224}\text{Ra}$ is the inadequacy of existing bifunctional chelators. ^{211}At is one of the most important alpha-emitting radionuclides that has been extensively studied in *in vivo* cancer models.⁶⁹ Not only does a sufficiently long half-life allow multiple synthetic procedures but it also produces only one α particle per decay, which simplifies dosimetry calculations and minimizes unwanted dose distribution of daughter products. ^{211}At can be produced in cyclotrons by the nuclear reaction $^{209}\text{Bi}(\alpha, 2n)^{211}\text{At}$ without involving nuclear fuel material as a target. Another important candidate is ^{225}Ac which emits four alpha particles per decay. However, the daughter products (^{221}Fr , ^{213}Bi , and ^{217}At) cause cytotoxicity to the healthy cells. The

main problem associated with alpha therapy is the release of multiple daughter radionuclides from the nanoplatform as the chemical properties of the parent and daughter radionuclides are generally not similar. Additionally, the recoil energies of the daughter radionuclides are very high compared to the strength of the chemical bonds. It is yet to be investigated in detail whether the daughter radionuclide stays in the nanoplatform after shooting out an α particle. Consequently, these daughter radionuclides might migrate to different healthy tissues and organs giving serious radiotoxicity effects.

Auger Electron Emitter

Auger electron arises when a radionuclide decays by electron capture (EC) or internal conversion (IC). During radioactive decay, when a vacancy is created in the inner electron orbital, it is filled by an outer shell electron. The energy difference created from this transition is transferred to another electron resulting in its final ejection from the atom. The ejected, low-energy electron is an Auger electron. On average, 5 to 35 Auger electrons are emitted per one decaying atom with energy ranges from a few eV to 1 keV. LET of these Auger electrons is 4–26 keV/ μm with a penetration range <0.5 μm in biological tissues. This maximizes the cytotoxic effect by breaking DNA double strands while generating reactive oxygen species (ROS).^{70,71} As maximum energy is deposited by Auger electrons adjacent to the decay site, the therapy requires precise dose delivery to the components inside the cells. The precise DNA double helix diameter, measuring 2 nm, exactly matches with the range of the maximum energy deposition by Auger electron.⁷² Due to this, Auger electrons are taken into consideration for the treatment of small tumors or clusters of cancerous cells. A list of Auger electron-emitting radionuclides is summarized in Table 3. Traditionally, palladium-103 (^{103}Pd)

Table 3. Physical Characteristics of Auger Electron Emitting Radioisotopes

Radionuclide	Half-life	Mode of decay ^a	Emission	Principal γ -component E in keV (% abundance)
^{111}In	2.8 d	EC (100%)	γ	245.4 (94.2)
^{125}I	60 d	EC (100%)	γ	35.49 (6.6)
^{103}Pd	16.9 d	EC (100%)	γ	20 (64)

^aOnly principal decay mode is mentioned; EC indicates decay by electron capture; E indicates energy.

and iodine-125 (^{125}I) have been used for low-dose rate brachytherapy since 1970.⁷³ Indium-111 (^{111}In) is another important radionuclide that has been used as a nanoscale brachytherapy agent. However, it is not suitable for internal RT due to emission of high-energy photons (>200 keV).²⁴

Beta (β^-) Particle Emitter

A β^- particle is a negatively charged high-energy electron emitted during nuclear decay process. β^- emitting radioisotopes are widely used in cancer treatment by means of internal RT. Nuclear decay characteristics of some beta emitters are listed in Table 4. Compared to alpha and Auger electron emitters, LET of β^- particle is much lower (0.1–1.0 keV μm^{-1}) and has a higher spatial penetration range which varies from 0.05 to 12 mm.⁷⁴

These long-range beta particles act as a double-edged sword. On one hand, they can travel through several cell diameters

Table 4. Physical Characteristics of β^- Emitting Radioisotopes

Radionuclide	Half-life	Mode of decay ^a	Energy (keV) ^b	Principal γ -component E in keV (% abundance)
¹³¹ I	8.0 d	β^- , γ	970.8	364.5 (81.2)
¹⁷⁷ Lu	6.7 d	β^- , γ	498.2	208.4 (11.0)
¹⁸⁸ Re	16.9 h	β^- , γ	2120.4	155.0 (14.9)
¹⁹⁸ Au	2.7 d	β^- , γ	1372.5	411.8 (95.5)
¹⁹⁹ Au	3.1 d	β^- , γ	452.6	158.4 (36.9)
⁹⁰ Y	64.1 h	β^-	2282.0	No γ -ray

^aOnly principal decay mode is mentioned; ^bFor β^- particles maximum β^- energy is mentioned.

which increases average dose to the tumor by breaking DNA and reactive oxygen species (ROS) generation, which permanently or partially arrests the cell cycle. This phenomenon makes them suitable candidates for treating bulky or large tumors. On the other hand, they also deliver doses to the surrounding healthy tissues.⁷⁵ Additionally, another limitation of beta radiation is that, similar to alpha particles, they cannot provide a lethal dose to a single cancerous cell.⁷⁶ However, the long-range crossfire effect gives beta radiation supremacy over targeted alpha therapy. As our current understanding relents, iodine-131 (¹³¹I), lutetium-177 (¹⁷⁷Lu), rhenium-188 (¹⁸⁸Re), gold-198,199 (^{198/199}Au), yttrium-90 (⁹⁰Y) have been researched in preparation of nanobrachytherapeutic agents.^{17,60,77,78} The nanocarriers which are composed by high Z materials enhance the radiation dose deposition by the radiosensitization mechanism.²⁴ Some of these beta emitting radionuclides also emit gamma photons, which helps visualize the distribution of radiolabeled NPs

within the body by employing gamma scintigraphy imaging system.

To make the best choice of the radionuclide, the size and position of the malignant tumor must be considered. As already discussed above, small clusters of tumors or bulky tumors require different radiation doses for effective ablation of cancer cells. Furthermore, the synthesis and the purification process should be in accordance with the half-life of the corresponding radionuclide.⁷⁹ Keeping the biochemical properties in mind, the uptake of radiolabeled NPs should be highest at the diseased site with minimal or no uptake in normal tissues or organs so that the radiation dose will only be delivered at the targeted site.

INTERNALIZATION PROCESS OF NPS

Cells internalize NPs by adopting endocytic pathways, having five distinct categories: macropinocytosis, caveolae-dependent endocytosis, clathrin-dependent endocytosis, phagocytosis, and clathrin or caveolae-independent pathways (Figure 4).⁸⁰ Clathrin-dependent endocytosis is one of the main pathways for internalizing NPs inside the cell which starts by binding the surface ligands of the NPs to the specific receptors of the cell membrane. NPs with a size of 100–500 nm internalize within the cell via this mechanism.⁸¹ The caveolae-dependent endocytosis pathway is applicable for the NP of size ranging from 50 to 100 nm.⁸² The particle-like viruses and NPs modified with cholera toxin B, SIV40, nucleic acid and cell-penetrating peptides can penetrate within cells independent of clathrin and caveolae-mediated pathways.^{83,84} Phagocytosis is a process by which immune cells eliminate diseased cells, pathogens or any other foreign material in our body. NPs are also cleared from the body via phagocytosis which poses a

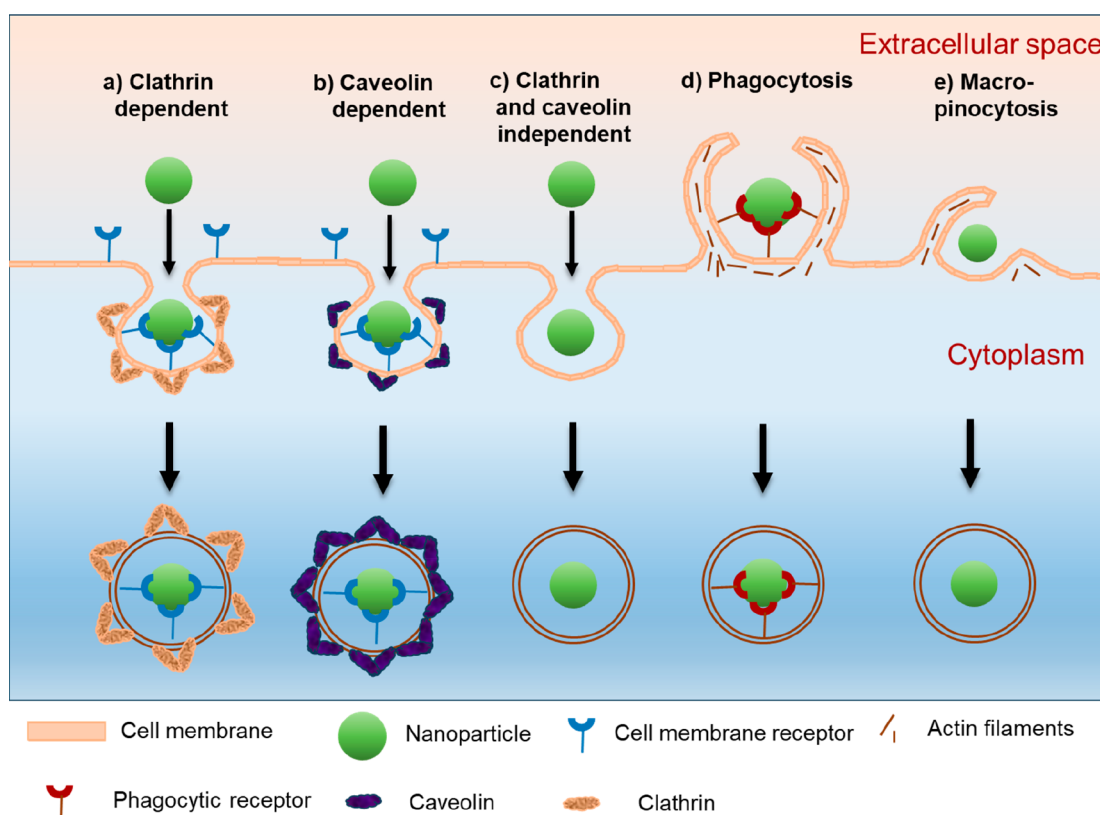


Figure 4. Schematic illustration of various pathways for uptake of NPs via endocytosis.

Table 5. Representative Examples of Nanoparticle Systems That Were Radiolabeled with Therapeutic Radionuclides for Use in Nanoscale Brachytherapy in Preclinical Settings

Serial No.	Radiolabeling method	Types of NPs	Radioisotope used	Targeting ligand	Tumor model	Tumor uptake (ID/g)	Reference
1	Chelation	Metal (Au@TADOTAGA)	²²⁵ Ac	Nontargeted	U-87 MG Glioblastoma	60.67% ± 3.87% (2 h p.i.) ^a	94
2	Adsorption	Metal (AuNP-S-mPEG)	²¹¹ At	Nontargeted	C6 glioma or PANC-1 (Pancreatic cancer)	-	95
3	Adsorption	Metal (AuNP-PEG-trastuzumab)	²¹¹ At	Targeted (Trastuzumab monoclonal antibody)	SKOV-3 (Breast cancer)	-	93
4	Chelation	Metal (Trastuzumab-AuNP- ¹¹¹ In)	¹¹¹ In	Targeted (Trastuzumab antibody)	HER-2 (breast cancer)	-	77
5	Adsorption	Metal alloy (¹⁰³ Pd:Pd@Au-PEG)	¹⁰³ Pd	Nontargeted	PC-3 (Prostate cancer)	-	96
6	Intrinsically radiolabeled	Metal alloy ([¹⁰³ Pd]AuPd)	¹⁰³ Pd	Nontargeted	CT26 (Colorectal cancer)	54 ± 13% (20 d p.i.)	97
7	Ion exchange	Metal (¹⁰³ Pd@Au)	¹⁰³ Pd	Nontargeted	PC-3 (Prostate cancer)	101.50 ± 23.72% (1 d p.i.)	23
8	Chelator free	Covalent organic framework (PEG-COF-Ag- ¹²⁵ I)	¹²⁵ I	Nontargeted	PC-3 (Prostate cancer)	61.674.0% (10 h p.i.)	98
9	Radiochemical doping	Core shell NPs (¹³¹ I-doped Ag-PEG)	¹³¹ I	Nontargeted	WI-38 (Lung cancer)	63.8 ± 1.3% (15 min p.i.)	99
10	Chelator free	Polymer (¹³¹ I-poly(N-isopropylacrylamide)	¹³¹ I	Nontargeted	PC-3 (Prostate cancer)	-	20
11	Chelator free	Superparamagnetic iron oxide NPs (¹³¹ I-CC49-APTES@SPIONS)	¹³¹ I	Targeted (CC49 monoclonal antibody)	LS174T (Colon adenocarcinoma)	-	100
12	Radioiodination	Elastin-like polypeptide (¹³¹ I-ELP)	¹³¹ I	Nontargeted	4T1 (Breast cancer)	-	101
13	Chelator free	Melanin NPs (MNP-Ag- ¹³¹ I)	¹³¹ I	Nontargeted	PC-3 (Prostate cancer)	-	102
14	Ion exchange	Metal oxide NP (¹⁷⁷ Lu-EuDPA/SiO ₂ -NH ₂)	¹⁷⁷ Lu	Nontargeted	HT-29 (Colorectal Cancer)	-	103
15	Chelation	Metal (¹⁷⁷ Lu-T-AuNP)	¹⁷⁷ Lu	Targeted (Panitumumab)	MDA-MB-468 (Breast cancer)	465.7 ± 135.6% (1 h p.i.)	104
16	Chelation	Metal nanostars (¹⁷⁷ Lu-DTPA-pAuNS)	¹⁷⁷ Lu	Nontargeted	SAS-3R (Head and neck carcinoma)	125.09 ± 27.26% (4 h p.i.)	22
17	Chelator free	Organic and inorganic NPs (¹⁸⁸ Re-Poly lactide, ¹⁸⁸ Re-SiO ₂ , ¹⁸⁸ Re-Au, ¹⁸⁸ Re-Fe ₃ O ₄ NPs)	¹⁸⁸ Re	Nontargeted	B16-F10 (Melanoma cancer)	92–97% (10 d p.i.)	105
18	Intrinsically radiolabeled	Cyclic RGD Conjugated Au NP	¹⁹⁹ Au	Targeted (RGD peptide)	B16-F10 (Melanoma cancer)	497 ± 56% (24 h p.i.)	60
19	Synthesis followed by irradiation	Gold dendrimer nanocomposites	¹⁹⁸ Au	Nontargeted	B16F10 (Melanoma cancer)	-	106
20	Intrinsically radiolabeled	Metal NP functionalized with gum arabic (GA- ¹⁹⁸ AuNP)	¹⁹⁸ Au	Nontargeted	PC-3 (Prostate cancer)	19.9 ± 4.2% (31 d p.i.)	107
21	Intrinsically radiolabeled	Metal (¹⁹⁸ AuNP-EGCG)	¹⁹⁸ Au	Targeted (Epigallocatechin-gallate)	PC-3 (Prostate cancer)	200% (24 h p.i.)	108
22	Intrinsically radiolabeled	Mangiferin functionalized AuNP (MGF- ¹⁹⁸ AuNP)	¹⁹⁸ Au	Nontargeted	PC-3 (Prostate cancer)	79.82 ± 10.55% (24 h p.i.)	109
23	Chelation	Polymer (⁹⁰ Y-Isp-PrPOZ)	⁹⁰ Y	Nontargeted	PC-3 (Prostate cancer)	-	110
24	Adsorption	Citrate coated superparamagnetic iron oxide NP	⁹⁰ Y	Nontargeted	CT-26 (Colon cancer)	-	111

^ap.i. indicates post injection.

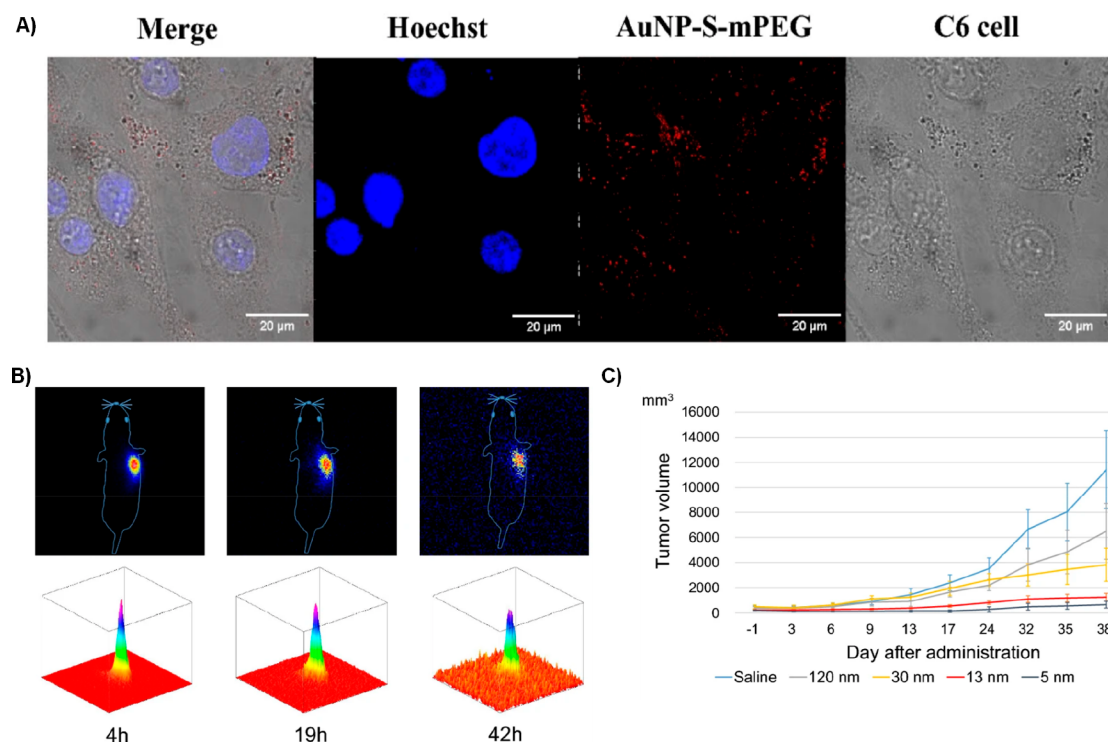


Figure 5. A) NPs uptake is shown when C6 glioma cells were incubated with 5 nm AuNP-S-mPEG NPs having concentration 138.4 mg/L for 24 h. The leftmost image is the bright field reflectance image of the cells, second section depicts the uptake of NPs by the cells, third section represents fluorescent Hoechst staining for DNA, and fourth section is the fused image. B) Scintigraphy of PANC-1 bearing mice at different time points after intratumoral administration of ²¹¹At-AuNP-S-mPEG of 13 nm diameter. The surface plots in lower rows represent square field of view of the dorsal detector with side length 15 cm. C) Change in tumor volume after intratumoral administration of radiolabeled NPs. The standard deviation is indicated by the error bars. Reprinted with permission from ref 95. Copyright 2021 Springer Nature.

challenge for the engineering of nanomedicines. Recent studies showed the NPs displaying “markers of self” surface ligands CD47 showed reduced phagocytic uptake of NPs.⁸⁵ The macropinocytosis process includes solutes and extracellular fluids being engulfed by the extension of the plasma membrane, which is stabilized by actin.⁸⁶

Internalization of NPs largely depends on the cell type and the plasma membrane of the cell, which creates a boundary to maintain the intracellular environment. Apart from this, surface morphology e.g., charge, shape, and size of the NPs also influence the cellular uptake. Discoidal shaped NPs exhibit enhanced penetration attributed to their unique migration dynamics in comparison to spherical NPs.⁸⁷ Generally, neutral and negatively charged NPs have lower rate of cellular uptake than positively charged NPs.⁸⁸

In 2012, Hao et al. investigated the intracellular localization of gold NPs of size 4.5 nm in living HeLa cells.⁸⁹ HeLa cells were incubated with Cy5-functionalized Au NPs at different temperatures. At 37 °C, a strong fluorescence signal was observed, whereas no signal was observed at 4 °C (endocytosis is blocked at this temperature), confirming endocytosis as a dominant pathway for internal uptake of NPs within cells. To further investigate the endocytosis mechanism, the clathrin-mediated endocytosis path was blocked by preincubating cell lines with sucrose and the caveolae-mediated path was blocked by the addition of methyl- β -cyclodextrin. A hypertonic solvent, that can disrupt clathrin coated vesicles, was added to sucrose treated cell lines. Consequently, a notable lack of reduction in Au NPs uptake was observed. Methyl- β -cyclodextrin is a type

of drug that destroys domains formed by cholesterol through the inhibition of cholesterol synthesis or by removing cholesterol from the cell membrane. Ultimately, this impedes the caveolae mediated endocytosis process for NP internalization. Altogether these blocking experiments confirmed the internalization of Au NPs through the caveolae mediated endocytosis route.⁸⁹

Ng, et al. explored internalization pathways of Au NPs with 20 nm diameters, coated with fetal bovine serum, in MRC5 lung fibroblasts and Chang liver cells by various inhibitors and quantitatively analyzing through the ICP-MS technique.⁹⁰ When Au NPs were incubated with concanavalin A treated MRC5 lung fibroblasts cells, the cell uptake was reduced by 18.2% compared to control cells. Additionally, the uptake of Au NPs in Chang liver cells reduced by 17% following pretreatment with chlorpromazine. The reduction is due to inhibiting translocation of clathrins, as well as their adapter proteins from plasma membrane to vesicles located at intracellular levels. In contrast, the use of nystatin, known to inhibit caveolae-mediated NP internalization route by hindering the uptake of albumin and glycosphingolipids, as pretreatment showed no observable reduction in the uptake of Au NPs within the cells. Altogether, aforementioned experiments collectively substantiate that the uptake of Au NPs is solely dependent on clathrin dependent endocytosis pathway for both cell types of different origins.⁹⁰

A 2014 study, Bannunah et al. describes how the different surface charges of NPs affects the internalization process in two different epithelial cell lines namely CaCo-2 (human colon

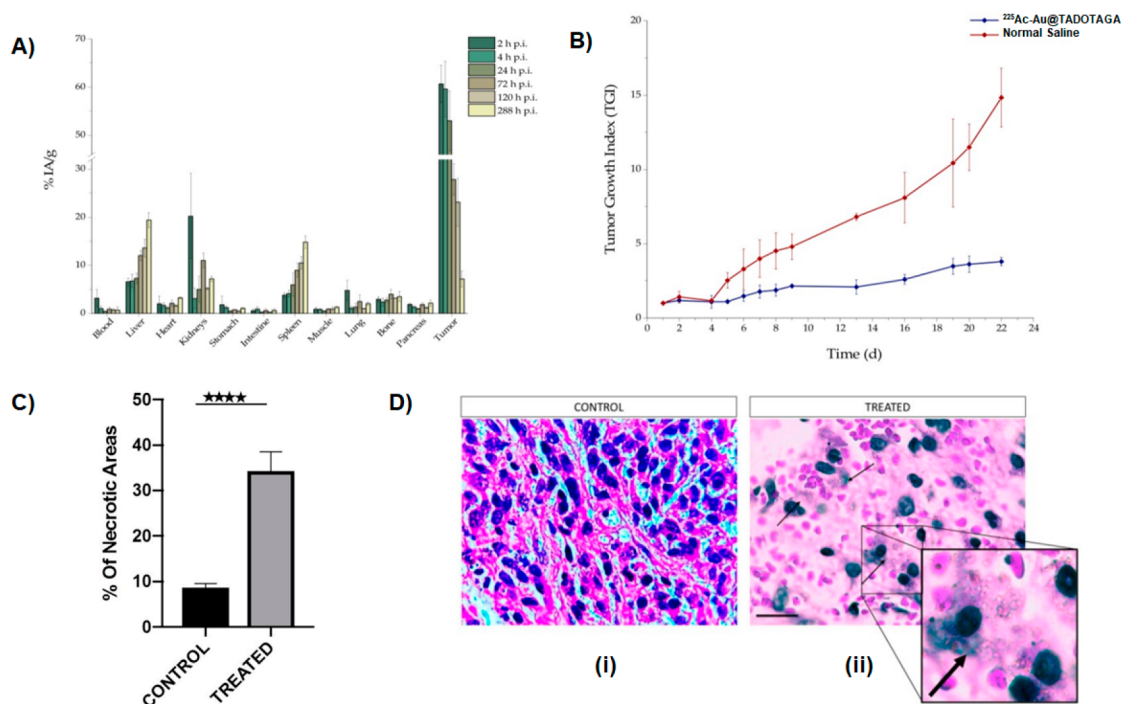


Figure 6. A) Biodistribution pattern after intratumoral administration of $[^{225}\text{Ac}]^{225}\text{Ac-Au@TADOTAGA}$. B) Representation of tumor growth index of controlled and treated mice after intratumoral injection. C) Necrotic area percentage of tumor. Four stars represents the p value (0.0001). D) H&E-stained image of controlled and treated tumor slices (100 \times magnification). The arrow shows NPs present in the necrotic lesions area. Reprinted with permission from ref 94. Copyright 2020 MDPI.

carcinoma) and Calu-3 (human airway).⁹¹ In accordance with their observation, positively charged NPs showed a higher level of toxicity due to the production of ROS and damaged mitochondria, whereas the negatively charged NPs did not exhibit the same effects. When clathrin-mediated endocytosis inhibitors were used, cellular uptake and transport were reduced to 46% and 38% respectively in the case of positively charged NPs. Contrarily, negatively charged NPs did not encounter any such difficulties. Likewise, EIPA (amiloride), a macropinocytosis inhibitor, also decreased in cellular uptake of the positively charged NPs. In the same study, it was observed that the uptake of positively charged NPs occurred at a faster pace in comparison with negatively charged NPs of similar size. The plasma membrane present in epithelial cells are made of negatively charged protein components; therefore, an electrostatic interaction arises between the positively charged NPs and negatively charged plasma membrane promoting cellular uptake in the endocytic system.⁹¹

PRECLINICAL STUDIES

In recent years, exploration of alpha, beta and Auger electron emitting radioisotopes in the development of injectable nanobrachytherapeutic agents has garnered much interest. An ideal nanoscale brachytherapy agent demonstrates high radiolabeling stability and excellent diffusivity at the tumor site for homogeneous distribution of radiation dose in the tumor volume while preventing gradual leakage of the radiolabeled NPs from the tumor. The process of leakage of radiolabeled NPs from the tumor would lead to accumulation of radioactivity in the healthy organs/tissues, which might pose radiotoxicity concerns. In this section, we provide a brief overview of the preclinical studies reported to date (most of which are summarized in Table 5).

Nanoscale Brachytherapy Using Alpha Emitting Radionuclides

Among the many alpha emitting radionuclides, ^{211}At shows excellent decay characteristics, potentially revolutionizing cancer therapy in forthcoming years.⁹² Dziawer et al. synthesized PEG modified gold NPs with a diameter of 5 nm and radiolabeled them with ^{211}At via chemisorption (labeling efficiency >99%).⁹³ They further modified the inactive NPs by attaching trastuzumab monoclonal antibody to target HER-2 which is overexpressed in human ovarian SKOV-3 cells. Reportedly, inactive trastuzumab modified AuNP-S-PEG bioconjugate successfully internalized in SKOV-3 cells preferentially near the nuclear area. Furthermore, cell viability decreased when 1.3 MBq mL⁻¹ (LD₅₀) of radio bioconjugate was administered.

In another study, Kato et al. synthesized ^{211}At labeled gold NP surface decorated with poly(ethylene glycol) methyl ether (mPEG) thiol of four different sizes (5, 13, 30, and 120 nm).⁹⁵ First, the cytotoxic effect was evaluated by incubating the C6 glioma cell lines with AuNP-S-mPEG for 24 h. The therapeutic efficacy was demonstrated by injecting a single dose of the nanoformulation intratumorally in C6 rat glioma cell tumor bearing rats and human PANC-1 tumor bearing mice. The distribution of the NPs was analyzed by scintigraphy and autoradiography techniques. The measurement of change in tumor volume continued for 39 days. AuNP-S-mPEG did not alter the cell viability when internalized, irrespective of the size of the NPs (Figure 5A). However, cell viability decreased significantly when both C6 rat glioma and PANC-1 were incubated with $^{211}\text{At-AuNP-S-mPEG}$ (diameter: 120 nm) having a radiation dose of 1 MBq/mL, implying that toxicity of the radiolabeled NPs is independent of cell type. $^{211}\text{At-AuNP-S-mPEG}$ remained at the site of administration and no

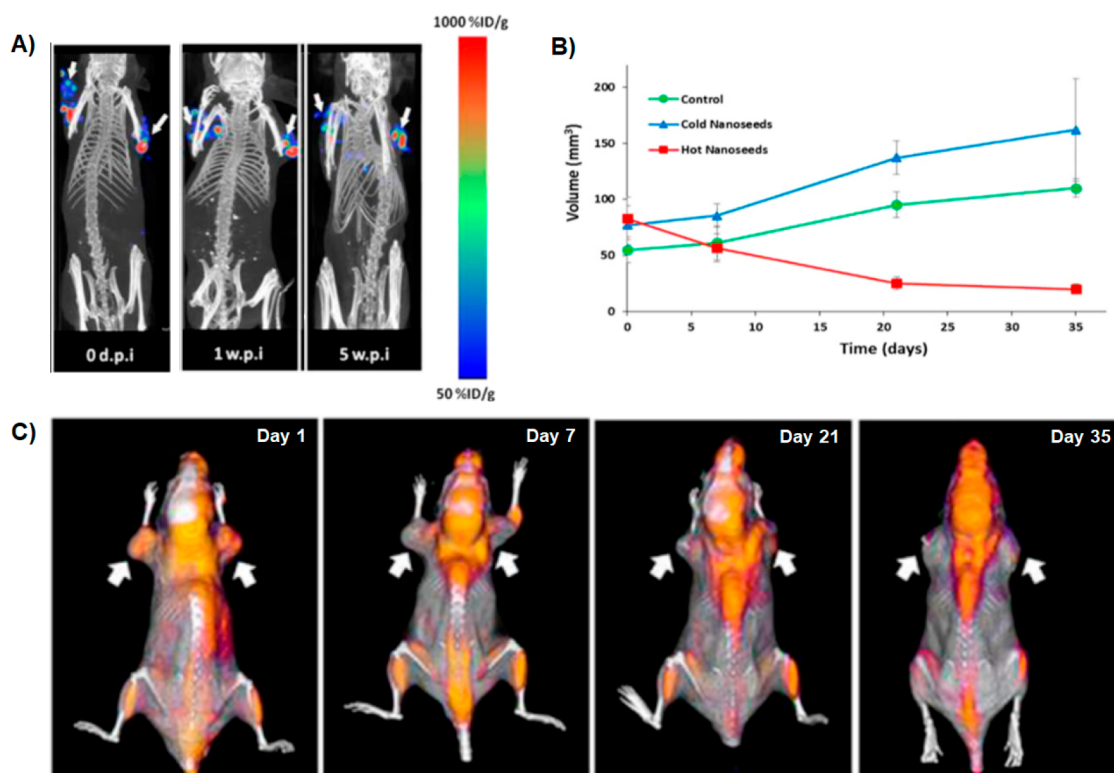


Figure 7. A) SPECT/CT imaging of retention of $^{103}\text{Pd}@Au$ nanoseeds in the tumor volume after 35 days of intratumoral injection in PC3-tumor bearing SCID mice. Tumors are indicated by white arrows. B) Graphical representation of change in tumor volume by CT scan analysis. C) Therapeutic efficacy of radiolabeled nanoseeds in PC3 tumor-bearing mice in serial ^{18}F FDG-PET/CT imaging showing reduction in ^{18}F FDG uptake in the tumor after 35 days. Tumors are indicated by white arrows. Reprinted with permission from ref 23. Copyright 2016 Springer Nature.

accumulation of free ^{211}At was observed in other organs except the tumor site, even after 42 h, nearly six ^{211}At half-lives (Figure 5B). The autoradiography of excised tumors revealed uneven distribution of the radiolabeled NPs having size 120 nm. However, 30 nm NPs distributed uniformly within tumor which implies that the diffusivity of NPs is probably size dependent. Tumor growth was arrested for both PANC-1 and C6 by ^{211}At -AuNP-S-mPEG represented in Figure 5C. The strongest effect was observed in case of ^{211}At -AuNP-S-mPEG having diameter of 5 nm.

^{225}Ac is another alpha emitting radionuclide that gained attention in targeted therapy and has recently been used as a nanobrachytherapeutic agent by Salvanou and co-workers.⁹⁴ They synthesized 5 to 9 nm Au NPs radiolabeled with ^{225}Ac by using a DOTA based chelators (TADOTAGA). ^{225}Ac -Au@TADOTAGA was stable in aqueous medium due to the strong bond formation between the chelators and AuNPs. This radiolabeled nanoformulation was injected both intratumorally and intravenously in U87MG bearing SCID mice. The biodistribution experiment revealed high tumor uptake ($60.67\% \pm 3.87\% \text{ IA/g}$) 2 h after intratumoral injection. However, a reverse trend was observed after 228 h: a decrease in tumor uptake ($5.21\% \pm 1.26\% \text{ IA/g}$) with an increase in spleen and liver uptake (Figure 6A). This is due to the recirculation of the NPs in the bloodstream and gradual release of ^{225}Ac . As a proof of concept, treatment studies were carried out which showed that the tumor growth index of treated mice after 22 d of injection was lower compared to their controlled counterpart (Figure 6B). Histopathology study of treated mice exhibited enhanced necrosis of tumor tissue with negligible effect on the peripheral tissue (Figure 6C and 6D). In the same

study, the intravenous injection of radiolabeled NPs revealed that accumulation of NPs occurred mainly in the liver, spleen, and kidney confirming hepatobiliary clearance. Although tumor uptake increased after 2 h of intravenous injection due to the enhanced permeability and retention (EPR) effect, radioactivity started to decrease after 120 h due to clearance of NPs through the hepatobiliary route and the release of ^{225}Ac from chelator. The ineffective chelation of ^{225}Ac with DOTA derivatives leads to questionable suitability for chelating the daughter products of ^{225}Ac .

Nanoscale Brachytherapy Using Auger Electron Emitting Radionuclides

Nanoscale brachytherapy using Auger electron emitters was first reported by Moeendarbari et al. in 2016.²³ A monodisperse layer of ^{103}Pd was coated onto spherical gold shells, whereby $^{103}\text{Pd}@Au$ nanoseeds (with diameter of ~ 120 nm) were synthesized. These nanoseeds were intratumorally injected into mice bearing prostate cancer tumors to assess their therapeutic efficacy and biodistribution *in vivo*. In order to achieve an even distribution of the radiation dose throughout the tumor mass, the intratumoral injection was carried out at six to nine sites with radioactivity totaling 55.5 MBq injected in each tumor. The retention evaluation of nanoseeds within the tumor volume and their migration to other organs was performed by an *ex vivo* biodistribution study with SPECT/CT imaging. The SPECT/CT imaging exhibited $101.50 \pm 23.72\% \text{ ID/g}$ retention of $^{103}\text{Pd}@Au$ nanoseeds within the treatment volume after 1 day post injection which increased to $274.5 \pm 77.6\% \text{ ID/g}$ after 5 weeks (Figure 7A), whereas minimal uptake of radioactivity was observed in the spleen and liver. *Ex vivo* biodistribution also corroborates with

the result obtained from SPECT/CT imaging. Moreover, tumor volume decreased up to 75% over the course of the treatment in comparison to the control and cold nanoseeds treated mice (Figure 7B). Therapeutic efficacy was assessed by [^{18}F]FDG-PET/CT scanning (Figure 7C) which also confirmed reduction of [^{18}F]FDG uptake at the tumor volume after the course of treatment.

Fach et al. reported preparation of [^{103}Pd]AuPd NPs, measuring 20 nm, synthesized from [^{103}Pd]PdCl₂ “hot precursor” and tetrachloroaurate tetrahydrate “cold precursor” followed by encapsulation with poly(*N*-isopropylacrylamide) polymer to enhance biodegradability.¹¹² This nanoformulation was injected intratumorally in CT26 colorectal tumor bearing mice. A delay in tumor growth was observed within first 10 days of dose administration (Figure 8). Additionally,

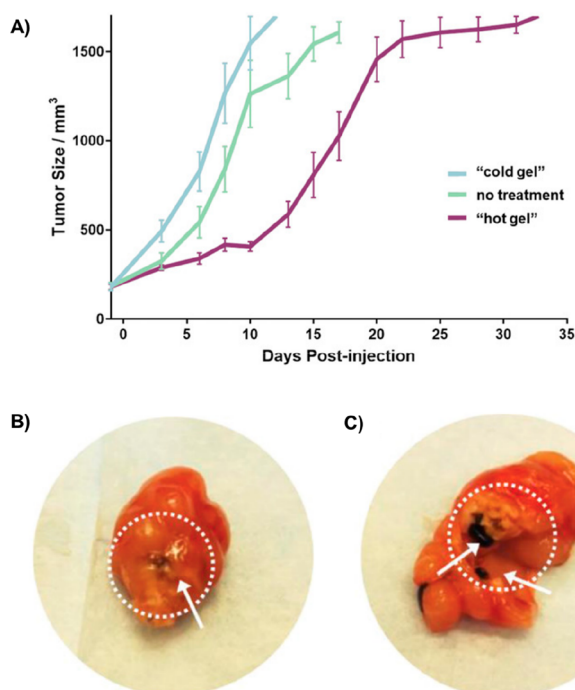


Figure 8. A) Therapeutic efficacy of mice treated with radioactive [^{103}Pd] AuPd (depicted in violet color) and nonradioactive (depicted in blue color) NPs. B) Image of tumor tissue (The white arrow indicates visible ^{103}Pd nanogel). C) The white arrow indicates separated radiolabeled nanogel inside the tumor and no further growth of tumor near the point of injection. Reprinted with permission from ref 112. Copyright 2021 Wiley.

biodistribution results revealed $54 \pm 13\%$ ID/g uptake in tumor site after 20 days and less than 0.01% ID/g of nanoformulation was found in other organs such as the kidney, liver, spleen, and muscle ensuring excellent *in vivo* stability. Therefore, the authors claimed [^{103}Pd]AuPd NPs as a potential replacement to the conventional brachytherapy seeds.

^{125}I is another important Auger electron emitting radioisotope. In a recent report, Zhang et al. used covalent organic framework (COFs) to synthesize ^{125}I labeled NPs.⁹⁸ First, an Ag⁺ ion was attached to the 2,2'-bipyridine-based COF followed by functionalizing with PEG, radiolabeling with ^{125}I within a remarkably short period of time (30 s). This resulted in PEG-COF-Ag- ^{125}I NPs with 94% radiolabeling yield and >90% stability in PBS and serum medium after 7 days. The authors reported that PEG-COF-Ag- ^{125}I NPs decreased the

survival rate by 25.8% on PC-3 cell lines. Additionally, the therapeutic efficacy of the radiolabeled NPs was estimated by intratumorally injecting 37 MBq of PEG-COF-Ag- ^{125}I NPs and evaluated by SPECT/CT at different time points (0.5, 10, 24, and 36 h p.i.). After 0.5 h, p.i., signal intensity was 3.2 times higher at tumor volume compared to the mice treated with only ^{125}I . The retention of PEG-COF-Ag- ^{125}I NPs was 61.67% in the tumor volume. Furthermore, tumor volume also reduced by 63% in comparison with the initial size. However, optimizing the retention of the radiolabeled NPs in the tumor volume is crucial for enhanced efficacious therapy.

Cai et al. synthesized Au NPs radiolabeled with another well-known Auger electron emitter, ^{111}In , which was attached with AuNPs by using DTPA.⁷⁷ The NPs were also functionalized with PEG linked with trastuzumab to obtain trastuzumab-AuNP- ^{111}In . The therapeutic efficacy and cell cytotoxicity of the radiolabeled NPs were demonstrated by intratumorally injecting 10 MBq of the radiolabeled NPs into subcutaneous HER2-overexpressing breast cancer tumor bearing mice and HER2-positive breast cancer cells, respectively. A tumor regression study was performed in a time period of over 70 days and it was observed that the tumor growth was arrested in the treated group, whereas the tumors grew up to 8-fold in the untreated group. However, no information about the retention of the radiolabeled NPs was provided in this study.

Nanoscale Brachytherapy Using β^- Particle Emitting Radionuclides

^{177}Lu is widely recognized as a therapeutic isotope and has been extensively explored within the radiopharmaceutical industry.⁷⁸ Yook et al. synthesized PEG modified panitumumab functionalized Au NPs radiolabeled with ^{177}Lu using a DOTA-based chelator.¹⁰⁴ Panitumumab is an antibody which targets the epidermal growth factor receptors (EGFRs), which is overexpressed in breast cancer (BC) cells. The aim of the study was to evaluate the therapeutic efficacy of the radiolabeled NPs in an MDA-MB-468 human BC model. Single doses, each of 4.5 MBq of targeted panitumumab- ^{177}Lu -AuNP and nontargeted ^{177}Lu -AuNP were intratumorally administered into different groups of tumors (BC) bearing mice. Both targeted and nontargeted NPs arrested the tumor growth after 90 days. However, the tumor growth was inhibited more in the targeted group in comparison to its nontargeted counterpart. The SPECT/CT imaging at 1 and 48 h p.i. demonstrated the retention of the NPs (Figure 9A). An *ex vivo* biodistribution study demonstrated that the uptake of both targeted and nontargeted NPs was >300%–400% ID/g in the tumor volume after 1 h p.i., whereas >3% ID/g radioactivity was accumulated in liver and spleen (Figure 9B). Therefore, no major tumor retention impact for either targeting or nontargeting ^{177}Lu labeled NPs was observed.

Lin et al. also synthesized PEG modified Au nanostars (AuNS); however, they used DTPA as a chelator for radiolabeling ^{177}Lu , which resulted in ^{177}Lu -DTPA-pAuNS.²² The authors evaluated the therapeutic efficacy of the radiolabeled NPs by intratumorally injecting both ^{177}Lu -DTPA-pAuNS and ^{177}Lu -DTPA in head and neck squamous cell carcinoma (HNSCC) bearing mice. The SPECT/CT imaging and *ex vivo* biodistribution analysis (Figure 10) showed the retention of ^{177}Lu -DTPA-pAuNS in the tumor volume up to 15 days, whereas the uptake of ^{177}Lu -DTPA in tumor was undetectable after 24 h p.i. Additionally, the tumor

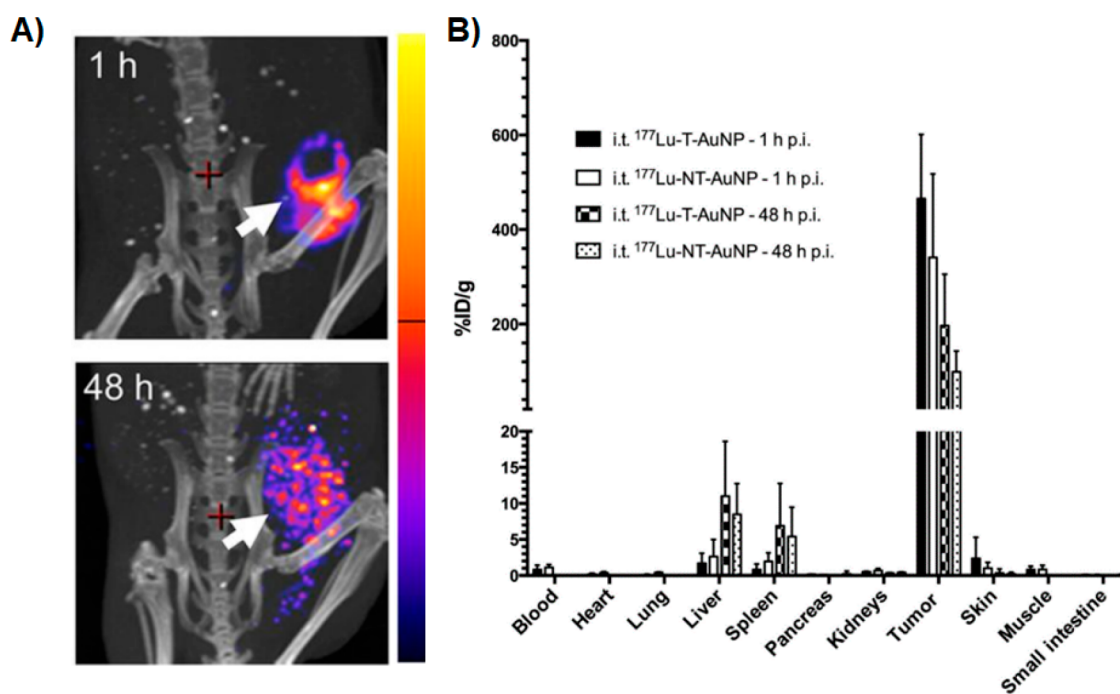


Figure 9. A) SPECT/CT images of MDA-MB-468 human BC tumor bearing mice at 1 or 48 h after intratumoral injection of ¹⁷⁷Lu-T-AuNP. B) *Ex vivo* biodistribution after intratumoral injection of ¹⁷⁷Lu-T-AuNP and ¹⁷⁷Lu-NT-AuNP in tumor bearing mice. Reprinted with permission from ref 104. Copyright 2016 Society of Nuclear Medicine and Molecular Imaging.

growth was arrested significantly in case of ¹⁷⁷Lu-DTPA-pAuNS in compared to ¹⁷⁷Lu-DTPA.

A study performed by Viana et al. developed a novel EuDPA/SiO₂-NH₂ NP by complexing Eu³⁺ with pyrimidine-2,6-dicarboxylic acid (DPA) followed by insertion in amino functionalized mesoporous silica NPs.¹⁰³ ¹⁷⁷Lu was then incorporated in EuDPA/SiO₂-NH₂ NPs by replacing Eu³⁺, and up to 93% of the radioactivity was incorporated. These radiolabeled NPs have been used for SPECT imaging as well as radiotherapy. As a result, radiolabeled NPs were intratumorally injected in an HT-29 mouse model of colorectal cancer. SPECT image confirmed the retention of the NPs (>70%) in the tumor site after 48 h of administration. After 5 weeks, tumor growth was inhibited significantly in the mice group treated with ¹⁷⁷Lu-EuDPA/SiO₂-NH₂. In comparison to the group treated with nonradioactive NPs, ¹⁷⁷Lu-EuDPA/SiO₂-NH₂ NPs are potential nanobrachytherapeutic agent. The author did not mention the radioactive dose administered, which encourages the evaluation of a detailed *in vivo* study for biological safety and radiation dose calculation.

After ¹⁷⁷Lu, most of the reported articles in nanobrachytherapy use ¹³¹I as the primary radioisotope. The first report was published by Hruby et al. in 2011.²⁰ The authors studied the dose-dependent therapeutic efficacy of ¹³¹I labeled poly(*N*-isopropylacrylamide) thermoresponsive polymer. Radiolabeling was achieved by the conventional chloramine T method. The therapeutic efficacy of the radiolabeled polymer was evaluated by intratumorally injecting two different doses, measuring 2 and 25 MBq, in human prostate cancer tumor bearing mice. The lower dose inhibited tumor growth, similarly, the higher radioactive dose reduced the tumor volume, and two out of six mice were completely cured. In both cases, no inflammation was observed.

Sheng et al. chosen melanin which is an integral part in human eyes, skin, hair to synthesize melanin NPs (MNPs) and

labeled with ¹³¹I.¹⁰² The radiolabeling was executed in two steps. First, chelation of Ag⁺ ions by MNPs followed by radiolabeling with ¹³¹I to form MNP-Ag-¹³¹I NPs of 6 nm diameter with 99% radiolabeling yield. No cytotoxicity was observed when MNP-Ag-¹³¹I NPs was incorporated in PC-3 prostate cancer cell lines. In order to determine the therapeutic efficacy of MNP-Ag-¹³¹I NPs, three groups of mice were intratumorally injected with 37 MBq MNP-Ag-¹³¹I NPs, PBS, and ¹³¹I. SPECT and Cherenkov radiation imaging confirmed the retention of the NPs after 8 h. On the third day, 18.5 MBq of MNP-Ag-¹³¹I was again administered intratumorally. After 7 days of observation, the mice were euthanized and it was observed that the tumor volume of the group treated with MNP-Ag-¹³¹I reached the equal of initial volume, whereas tumor volume increased up to 1.5 times larger in the other two groups. Therefore, MNP-Ag-¹³¹I NPs could be used for SPECT and Cherenkov radiation imaging and internal radiotherapy.

In another study, Stanković et al. prepared flower-shaped superparamagnetic iron oxide NPs (SPIONs) with 40 nm diameters and radiolabeled with ¹³¹I by CC49 antibody attached to SPIONs through the utilization of reactive groups present in 3-aminopropyltriethoxysilane (APTES).¹⁰⁰ The heating efficiency of SPIONs was evaluated for magnetic hyperthermia therapy and radiotherapy. The therapeutic efficacy was evaluated by administering the NPs intratumorally in LS174T human colon adenocarcinoma xenografts in NOD-SCID mice. SPECT imaging displayed retention of ¹³¹I-CC49-APTES@SPIONs in the tumor site even after 14 days of intratumoral injection. The combination of both hyperthermia and radiotherapy was most effective in suppressing tumor volume after 14 days of treatment with 73% tumor volume inhibitory rate (TVIR), whereas TVIR were 54.38% and 68.77% in the cases of hyperthermia and radiotherapy, respectively. Histopathological analysis disclosed severe

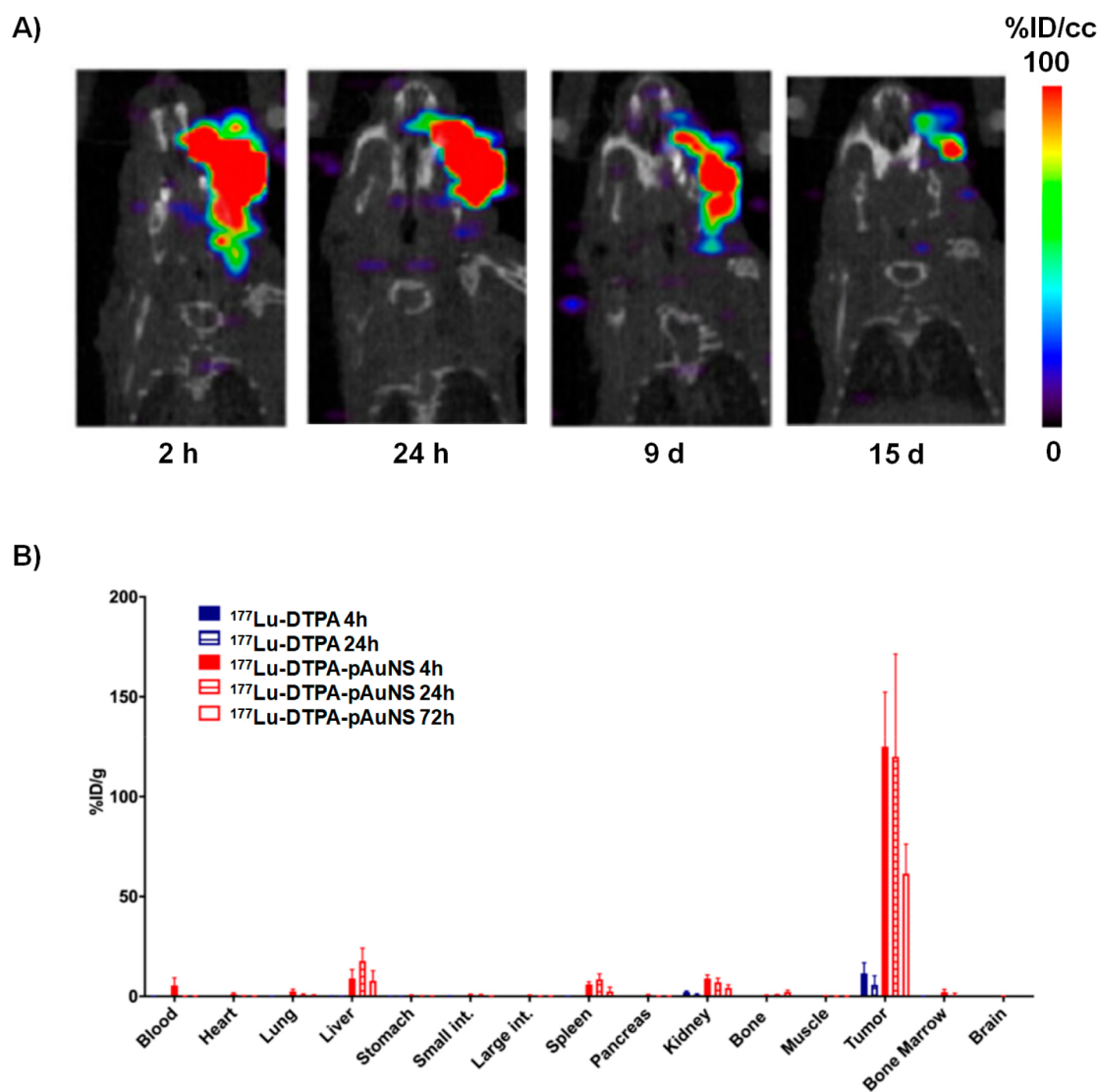


Figure 10. A) The micro-SPECT/CT images after intratumoral administration of ^{177}Lu -DTPA and ^{177}Lu -DTPA-pAuNS in HNSCC tumor-bearing mice. B) *Ex vivo* biodistribution evaluation of ^{177}Lu -DTPA and ^{177}Lu -DTPA-pAuNS after intratumoral administration in HNSCC tumor-bearing mice ($n = 4$). Reprinted with permission from ref 22. Copyright 2021 MDPI.

necrosis and hemorrhaging in the tumor tissues of mice that have been treated with combined therapy of hyperthermia and radiation. Although the combined therapy is a better choice, ^{131}I -CC49-APTES@SPIONs preferentially stayed at the injection site and did not reach in the broader area, which minimized the therapeutic effect. Therefore, a higher-energy β^- emitting radionuclide like ^{90}Y with high radioactive dose along with repetitive treatment may be a better choice.^{113,114}

In a recent study, Kelly et al. combined nanoscale brachytherapy and immunotherapy to enhance the treatment efficacy of metastatic disease.¹⁰¹ The authors synthesized elastin-like polypeptides (ELPs) with an oligolysine tail (ELP-K12) where ^{131}I radionuclide conjugated to Tyr residues at the C-terminus and CpG formed complex electrostatically with C-terminus of an ELP. Both the conjugates were intratumorally injected in lung cancer 4 T1 bearing BALB/c mice where the conjugate ELP-K₁₂/CpG undergoes an LCST phase transition to form ELP depots in normal body temperature. The retention of ^{131}I was enhanced within the tumor volume due to cross-linking of the ELP. As a result, the radionuclide irradiated the tumor cells from the inside, along with

systematic release of CpG from the depot. This substantially activated immune signaling within the tumor. This synergistic therapeutic approach not only decreased the tumor volume but also increased the survival rate of the mice.

AuNPs are well-known “radiosensitizers” in oncology as they can enhance the radiation effect in biological tissues in the presence of radioactivity. Few reports where both ^{198}Au and ^{199}Au are used for radiolabeling have been discussed.^{59,60} Khan et al. prepared radioactive polymerized gold dendrimer (poly- ^{198}Au) NPs by forming dendrimer-amine[AuCl_4] complex consequently reducing Au^{3+} to Au^0 .¹⁰⁶ The particle size of the NPs ranges from 10 to 29 nm. [$^{197}\text{Au}^0$] gold-dendrimer was irradiated in a nuclear reactor by neutron beam to obtain (poly- ^{198}Au) nanocomposites. The therapeutic efficacy of this radioactive nanocomposite was evaluated by intratumoral administration of two different doses (1.3 MBq and 2.7 MBq) in B16F10 melanoma tumor bearing C57BL/6J mice. Reduction of tumor growth was more pronounced in the group injected with the highest dose compared to the other groups. However, the authors did not perform biodistribution analysis

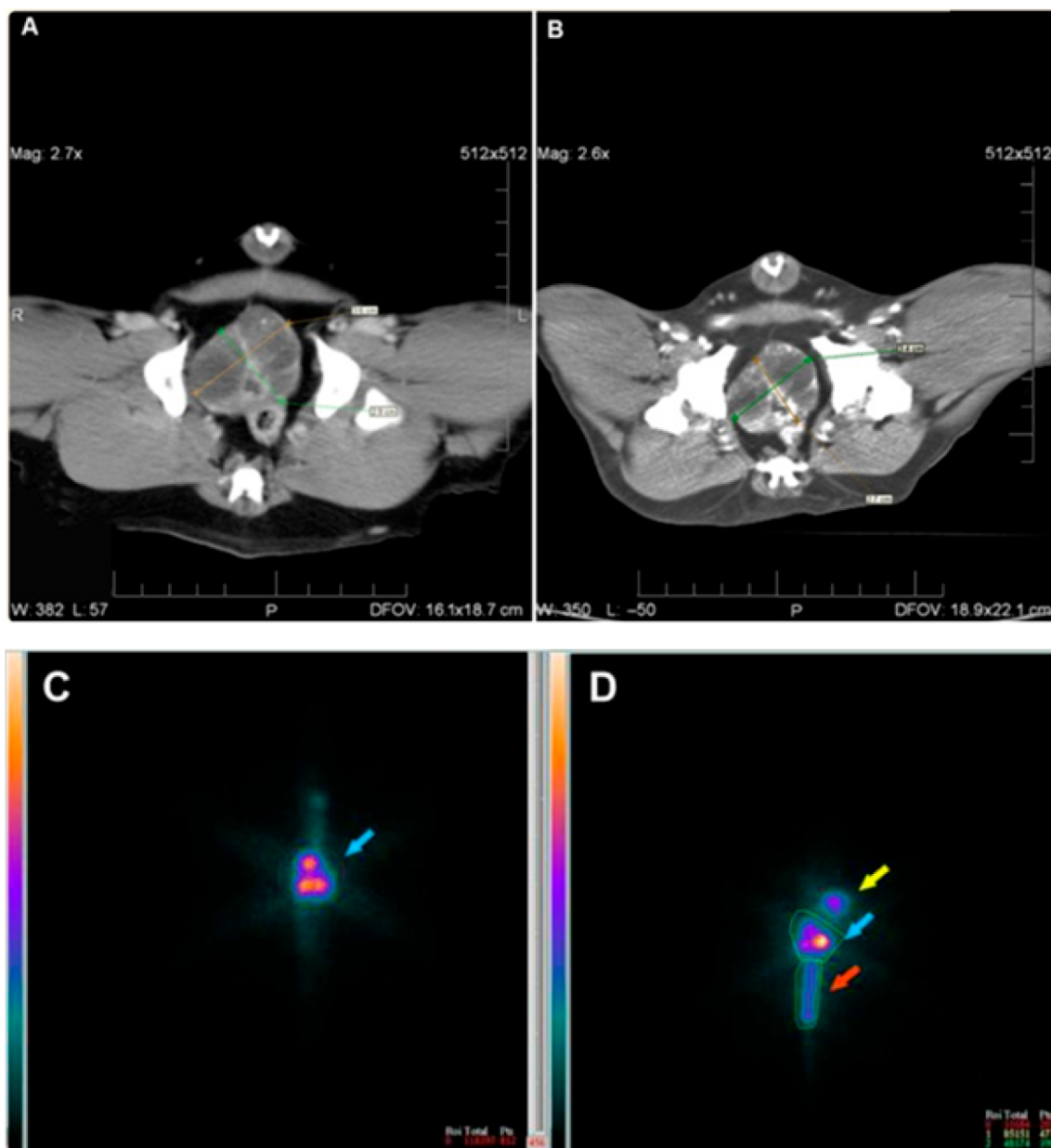


Figure 11. A) CT image of dog with prostatic carcinoma before injection. B) CT images of one representative dog treated with GA-¹⁹⁸AuNP showing 50% tumor volume reduction. (C-D) Representative scintigraphic images recorded after 30 min p.i. of GA-¹⁹⁸AuNP. Blue arrows indicate the presence of radioactive AuNP. Multiple injection points are visible within tumor volume. Yellow and red arrows indicate the uptake of small amounts of GA-¹⁹⁸AuNP in the bladder and urethra, respectively. Reprinted with permission from ref 115. Copyright 2014 Dove Press.

to monitor localization of radioactivity in the tumor and its leakage to other nontargeted organs.

Shukla et al. synthesized AuNPs which was functionalized with epigallocatechin gallate to form (EGCg)-¹⁹⁸AuEGCg measures sizes ranging from 40 to 50 nm.¹⁰⁸ EGCg is used to actively target laminin receptors (Lam 67R) overexpressed in prostate cancer cell lines. In this study, the authors investigated internalization procedure of ¹⁹⁸Au-EGCg in PC3 cell lines by endocytosis and assessed the therapeutic effect by intratumorally injecting 5 MBq of ¹⁹⁸Au-EGCg NPs to mice bearing the prostate tumor. After 24 h of injection approximately 72% of ¹⁹⁸Au-EGCg NPs were found in the tumor volume. The treated group was observed for 28 days, and the tumor reduced to 80% in comparison to the control group. The *ex vivo* biodistribution study, after day 42 post intratumoral injection,

indicated 34.7%ID retention of radiolabeled NPs in tumor, 2.5%ID in liver, and 18%ID in carcass.

A research group from University of Missouri synthesized gum arabic glycoprotein coated Au NPs and studied their therapeutic effect.¹⁰⁷ In a more advanced study, they attempted to determine the short-term safety profile of GA-¹⁹⁸AuNPs when injected intralesionally in canine models with prostate cancer.¹¹⁵ For this study, nine dogs were chosen and GA-¹⁹⁸AuNPs of doses 7.4 MBq/g of tumor tissue were injected. Complete blood parameters and urinalyses were performed routinely each week for one month. To assess the intratumoral retention scintigraphic imaging was recorded after 30 min of injection. CT images confirmed reduction in tumor volume (Figure 11A-B), although the results varied for each canine model. Scintigraphy images 30 min p.i. revealed on an

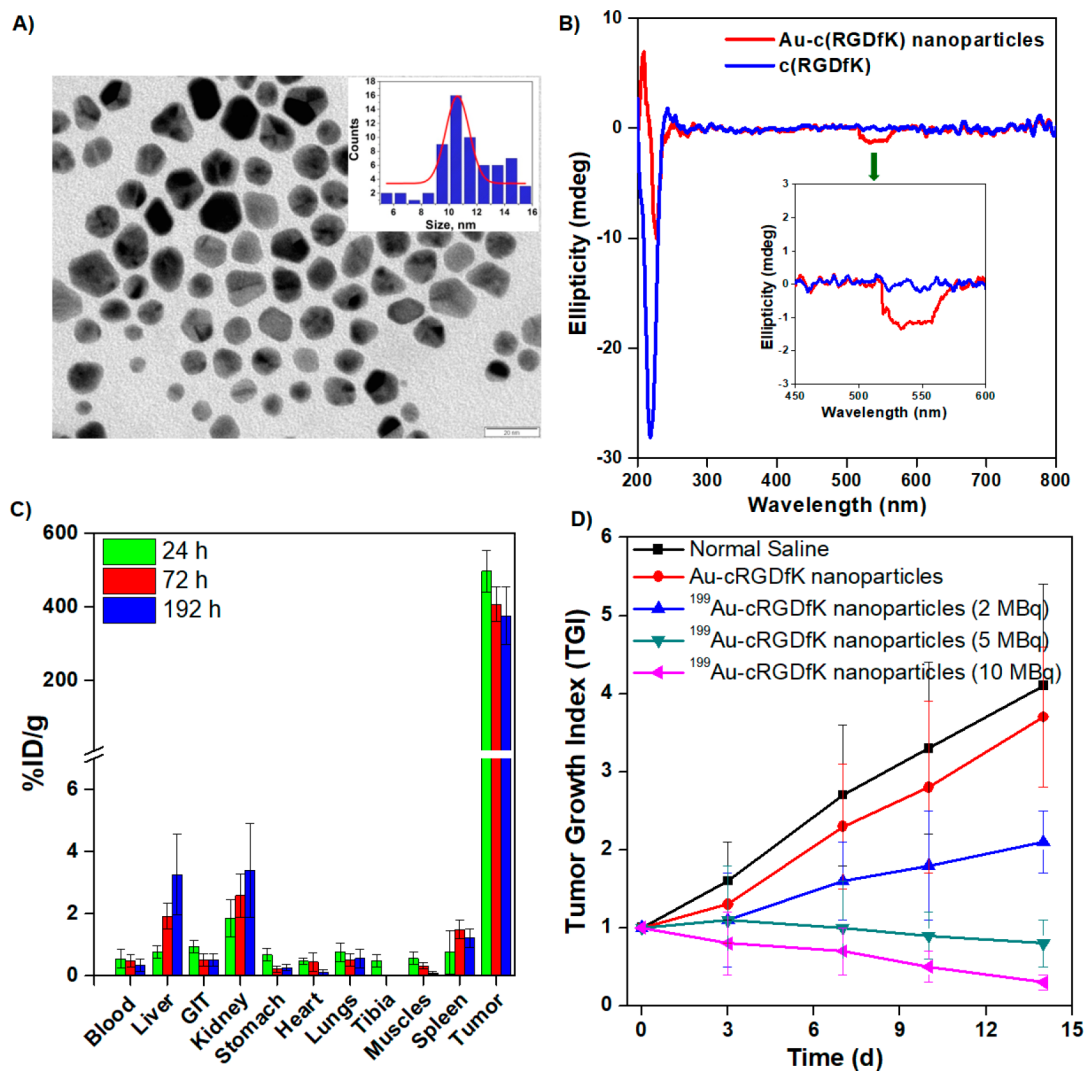


Figure 12. A) TEM image of AuNPs conjugated with cRGDfK NPs. B) Circular dichroism spectra of cRGDfK and AuNP conjugated with cRGDfK (inset: amplified view of CD spectra in 450–600 nm wavelength range). C) Biodistribution pattern of [^{199}Au]Au NPs conjugated with cRGDfK injected in tumor bearing mice. D) Effect of intratumoral injection (different doses) on the tumor growth index of tumor bearing mice. Reprinted with permission from ref 60. Copyright 2018 American Chemical Society.

average 53% of $\text{GA-}^{198}\text{AuNPs}$ remained in the tumor site. However, leakage was also observed in bladder and urethra (Figure 11C-D). There was no significant change in blood count and serum biochemistry between the before and after treatment values. The authors opined that since radioactivity retention in the tumor decreased, an in-depth study of dosimetry and toxicity was required before initiating phase I clinical trial.

The same group adopted green nano technology to synthesize mangiferin (MGF) encapsulated AuNP.¹⁰⁹ MGF is glucose functionalized xanthonoid abundantly found in mango peels. Here MGF is used as encapsulating material as well as a reducing agent. The core size of $^{198}\text{AuNPMGF}$ is 35 ± 2 nm with a hydrodynamic diameter of 55 ± 0.9 nm. The therapeutic efficacy was demonstrated by intratumorally injecting a single dose of 5.9 MBq $\text{MGF-}^{198}\text{AuNPs}$ in prostate cancer tumor bearing mice. After euthanization of the mice, $80.98 \pm 13.39\%$ tumor uptake at 30 min and $79.82 \pm 10.55\%$ at 24 h were observed whereas the liver uptake increased to $10.65 \pm 8.31\%$ at 24 h suggesting clearance of NPs through reticuloendothelial system. Due to the laminin receptor

specificity of MGF, enhanced accumulation in prostate cancer cell lines was observed. After 24 days of observation, the tumor volume decreased 2-fold with respect to the control group. Biodistribution studies after 24 days exhibited $60.96 \pm 25.56\%$ ID NPs remaining at tumor site, $13.00 \pm 10.97\%$ ID was observed in the carcass, and $1.44 \pm 2.97\%$ ID was observed in the liver with negligible uptake in other organs entitling $^{198}\text{AuNPMGF}$ as a promising nanobrachytherapy agent.

In another study, intrinsically radiolabeled [^{199}Au]Au NPs conjugated with cyclic RGD (cRGDfK) peptides were synthesized for targeting integrin $\alpha_v\beta_3$ receptors.⁶⁰ The cRGDfK peptide acted as both a reducing and stabilizing agent. The TEM images showed the size of the NPs was ~ 11 nm (Figure 12A). The circular dichroism (CD) spectra of the synthesized NPs showed peaks corresponding to the surface plasmon resonance (SPR) of the Au NPs (~ 535 nm). The notable observation of this CD peak is due to interaction of the dipole of the cRGDfK peptide with SPR of Au NPs (Figure 12B). The radiolabeled NPs were intratumorally administered in melanoma tumor bearing mice for nanoscale brachytherapy. Biodistribution studies revealed enhanced retention of radio-

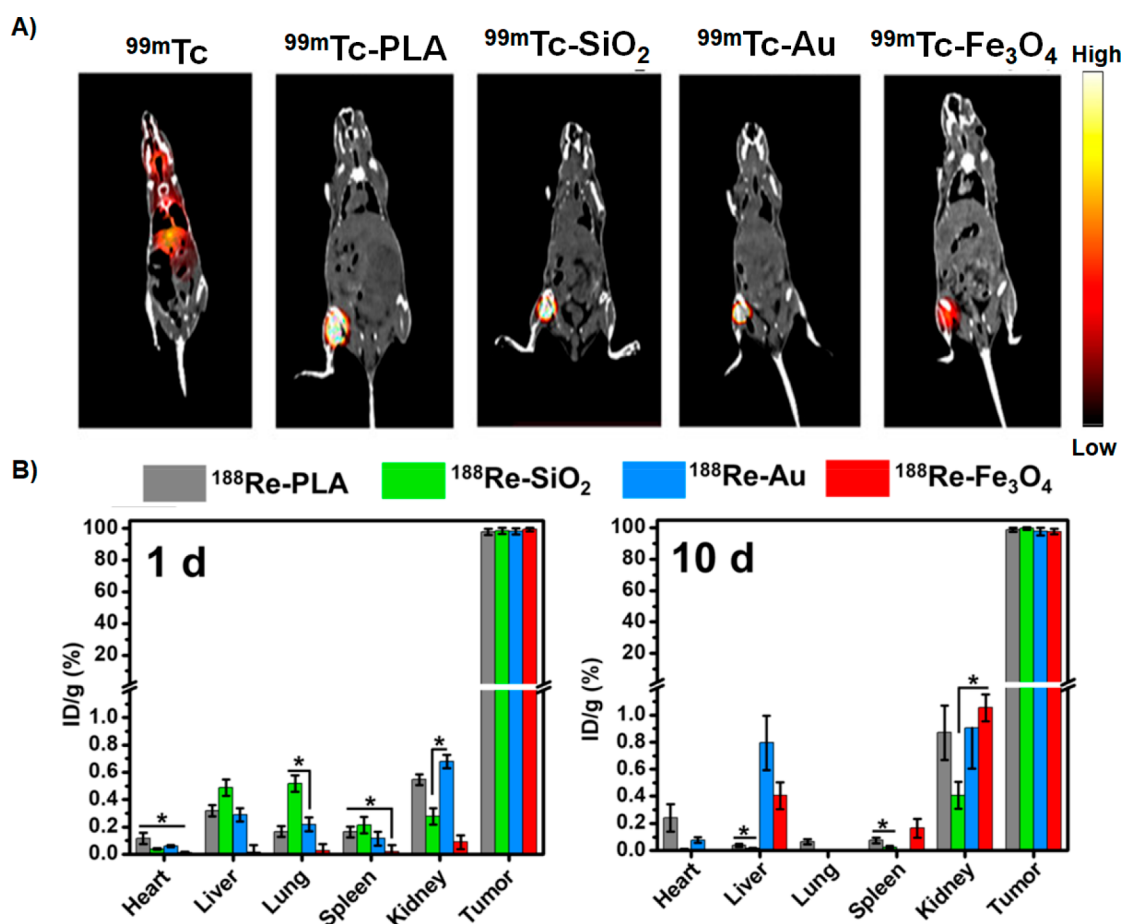


Figure 13. A) SPECT-CT images of the B16F10 melanoma-bearing mice treated with different ^{99m}Tc labeled NPs after 1 day. B) Direct radiometry analysis for tumors and various organs after the intratumoral injection of different ^{188}Re -labeled NPs in the B16F10 melanoma-bearing mice on the first and tenth day p.i. Reprinted with permission from ref 105. Copyright 2022 American Chemical Society.

activity at the tumor site over a prolonged period of time (Figure 12C). The treatment studies, performed by intratumoral injection of 5 and 10 MBq doses of radiolabeled NPs, demonstrated significant tumor regression with minimal changes in the mice's body weight (Figure 12D).

Karpov et al. adopted a universal chelator free approach for radiolabeling four different kinds of NPs which include polylactide (PLA), silica (SiO_2), gold (Au), and iron oxide (Fe_3O_4). These NPs are radiolabeled with ^{99m}Tc for diagnosis and with ^{188}Re for therapy.¹⁰⁵ To investigate the intratumoral retention, ^{99m}Tc labeled NPs were locally injected in a B16F10 melanoma tumor bearing CS7BL/6 mice. SPECT/CT images were recorded (Figure 13A) for 3 days, which revealed sustainable accumulation of NPs inside the tumor, whereas free ^{99m}Tc spread throughout the body. When ^{188}Re -labeled NPs (3 MBq) were injected intratumorally, 92–97% radioactivity remained in the tumor volume even after 10 days, regardless of the type of the NPs (Figure 13B). Furthermore, after 14 days of treatment ^{188}Re -labeled NPs were able to inhibit the tumor growth significantly and the mean survival rate of the treated animals resided in the range of 80–90%. According to the histological analysis of the tumor tissues, $^{188}\text{Re-AuNP}$ significantly damaged the tumor morphology, and its strong cytotoxic effect decreased the blood supply in tumor causing cell death.

Two reports were published where ^{90}Y was used in preparation for nanobrachytherapeutic agents. The first report

was published by Sano et al. in 2017.¹¹⁰ They synthesized different derivatives of a thermoresponsive biocompatible polymer, named polyoxazoline (POZ), labeled with ^{90}Y and ^{111}In by complexation with DOTA chelator. ^{111}In -labeled POZ derivatives were intratumorally injected in prostate cancer-implanted mice to evaluate overall localization and retention within the treatment volume. When the transition temperature of the polymer derivatives was less than $33.5\text{ }^\circ\text{C}$, 73.9% tumor retention was achieved after the first day of injection. The retention of NPs was directly proportional to the molecular weight of polymer i.e., Isp-PrPOZ (20 kDa). The therapeutic efficacy was determined by injecting ^{90}Y -Isp-PrPOZ intratumorally in human prostate cancer bearing mice. After 90 days, almost 50% mice survived.

Vukadinović et al. synthesized citrate coated, flower shaped, superparamagnetic iron oxide NPs (CA/SPIONs) labeled with ^{90}Y for dual magnetic hyperthermia and nanobrachytherapy to treat solid cancer.¹¹¹ The toxicity limit of CA/SPIONs was observed to be up to 1.0 mg mL^{-1} in mouse colon cancer cells. A single dose intratumoral injection of 0.25 mg nonactive NPs followed by a thirty-minute treatment of magnetic hyperthermia moderately increased the antitumor effect compared to the nontreated one. Conversely, intratumoral injection of ^{90}Y labeled CA/SPIONs in CT-26 (colon cancer) bearing mice displayed long-term retention in tumor volume with a significant decrease in tumor volume observed after 14 days of treatment, without any systemic toxicity. Hence, the authors

concluded that the limited effect of magnetic hyperthermia might be due to the inability of deep tissue penetration range. However, the combined effect was more effective for tumor therapy.

■ DOSIMETRY OF NANOSCALE BRACHYTHERAPY AGENTS

Radiation dosimetry is crucial for utilization of nanoscale brachytherapy agents in clinical context. It is essential to acquire dosimetry data to access the radiation safety of the radiolabeled NPs administered as well as to measure the effective radiation dose for internal radiotherapy. Prior to actual utilization in tumor therapy, accurate simulations of dosimetry of the nanoscale brachytherapy agents are essential in order to regulate the dose distribution within the tumor volume and the surrounding healthy organs/tissues. Radiation doses precisely absorbed in the healthy organs/tissues are determined by the rate of leakage of the administered radiolabeled NPs from the tumor site and their accumulation in these organs/tissues over a period of time. Physical characteristics of the radioisotopes such as half-lives, emission characteristics, and the retention time also contribute to radiation doses observed.¹¹⁶ To determine the radiation dose of the specified target organ, initially, the total cumulated radioactivity is calculated through integration of the time-radioactivity curve. Generally, Monte Carlo simulation techniques are used to accurately determine the energy or dose distribution within the region of interest. The overall pharmacokinetics of the nanoscale brachytherapy agents and their anatomical distribution are key points to calculating dosimetry. Although radiation dosimetry of nanoscale brachytherapy agents is essential for clinical translation, very few preclinical studies with dosimetry data have been reported to date.^{21,96,117,118} Overall, these preclinical dosimetry studies, using therapeutic radiolabeled NPs, could provide insight for basic treatment planning concerning the administration of therapeutic doses for future efficacious clinical studies.

■ POTENTIAL CLINICAL TRANSLATION OF NANOSCALE BRACHYTHERAPY AGENTS

While numerous published preclinical evaluations demonstrate the positive impact of radiolabeled NPs in nanoscale brachytherapy, their successful clinical translation is lacking. The primary reason remains the lack of knowledge regarding the exact radioactive dose of the radiolabeled NPs to be administered for maximal therapeutic benefit. This detailed dosimetry study must be performed in preclinical and clinical settings to determine the optimal dosage of the nanoscale brachytherapy agent for intratumoral injection. Also, the correlation or transition from preclinical data to clinical estimation should be investigated and validated. Another concern revolves around the toxicity effects of administered radiolabeled NPs for tumor therapy. Therefore, for *in vivo* applications, minimizing the amounts of nanomaterials employed will mitigate the concerns about potential risks associated with administering pharmacological amounts of nanomaterials to animals and human subjects. The use of biocompatible and biodegradable nanoplatfoms, coupled with the tracer technology used in formulating nanoscale brachytherapy agents, will undoubtedly help advance the translation of this treatment modality into clinical practice. Once the overall physiology and immune response are well

understood in small animal models using SPECT/PET imaging technologies, possibilities of comprehending the intracellular location of the radiolabeled NPs after endocytosis will be apparent. In addition to surface functionalization, the selection of intracellular molecules as targets has the potential to expand the horizons of nanoscale brachytherapy.

Ensuring optimal retention of radiolabeled NPs in the tumor following intratumoral injection is crucial for the therapeutic efficacy of the nanoscale brachytherapy procedure. Thus, its maximization is of paramount importance. This endeavor also minimizes the risk of irradiating healthy organs and tissues (especially liver and spleen) as a result of radiolabeled NP leakage from the tumor site. Inhomogeneous intratumoral radioactivity distribution might also raise concerns in certain cases.¹⁰⁴ The problem presents a conflicting solution: on one hand, the restricted diffusivity of the radiolabeled NPs limits the toxicity to the normal tissues/organs, while on the other hand, it deteriorates the dose distribution in the tumor required for maximum therapeutic benefit. A nanoformulation with enhanced diffusivity would improve homogeneity of the radiation doses in the tumor site but may also perform similarly to systemically administered agent. Thus, careful optimization is essential in establishing the best balance and ideal formulation. In addition to diffusivity of the NPs, leakage of radiolabeled NPs from the tumor post injection are also caused by irregular tumor vasculature, variable blood and lymph flow, and pressure gradients. Due to the individual nature of tumors, the percentage of leakage of radiolabeled NPs from the tumor site may vary from patient to patient. This further complicates treatment planning and dosimetric computations during the process of clinical translation. Though, it is desirable that the radiolabeled NPs should be retained in the tumor site over a prolonged period of time, the presence of such foreign substances in the body might also raise toxicity concerns. From this perspective, biodegradable nanoplatfoms are preferable for nanoscale brachytherapy applications. However, this necessitates use of the radio-nuclides with suitable half-lives for radiolabeling NPs and careful optimization of biodegradation parameters *in vivo* such that free radionuclides do not leach out of the degraded NPs and accumulate in nontargeted organs. Further considerations such as the size of the NPs, varying surface modification strategies, coinjecting biocompatible polymers that might sequester radiolabeled NPs within the tumor, and the use of different emerging radioisotopes may be worthwhile in pursuit of therapeutic optimization of nanoscale brachytherapy. Ultimately, structure-controlled manufacturing methods that enable cost-effective and robust routine production of nanoscale brachytherapy agents while adhering to the regulatory guidelines is an essential prerequisite toward their clinical translation.¹¹⁹ Despite all attributes, nanoscale brachytherapy is suitable only for treating primary tumors and not the metastatic sites. The restricts the use of this therapeutic modality for treatment of cancer in its early stages when extensive metastases have not occurred. Also, radiolabeled NPs are not an option when high dose rate (HDR) brachytherapy is required depending on the type of cancer.

■ CONCLUSIONS

The design and development of functionalized radiolabeled NPs for use in nanoscale brachytherapy has become a pressing requirement, rendering it a prominent and dynamic field of research in nano-oncology. In this review, we described the

latest advances in nanoscale brachytherapy analyzing their advantages compared to the conventional brachytherapy techniques. The success of this emerging clinical modality relies on the synthesis of functionalized and dispersible nanoplateforms with their robust radiolabeling strategy to achieve excellent radiochemical stability. The size, shape, charge, and functionality of the nanoplateform must be carefully optimized to achieve prolonged retention of the radiolabeled NPs in the tumor with minimal leakage and accumulation in the nontargeted organs. Different imaging modalities (SPECT/PET, MRI, CT, optical imaging, etc. either alone or in combination) can be synergistically applied based on the intrinsic properties of the radiolabeled NPs to visualize their uptake at the tumor site and monitor their therapeutic efficacy. Furthermore, for the clinical translation of nanoscale brachytherapy agents, systematic internal radiation dosimetry is imperative as a safety assurance by quantifying the expected dose at the tumor site. As dosimetry relies on the kinetics and clearance patterns of the intratumorally administered radiolabeled agents. Therefore, conducting detailed studies on kinetic modeling and biodistribution pattern revealing the influence of physicochemical and biological aspects of the synthesized nanoplateforms is of great importance. Owing to the relatively higher cost of nanoformulations, conducting cost effectiveness analyses must also be considered when devising the clinical translation strategies for nanoscale brachytherapy. In conclusion, it is envisaged that nanoscale brachytherapy shall be used in the future as an important treatment modality in clinical oncology. This advancement will create a highly productive and challenging field for academics, industry, clinicians, and regulators.

AUTHOR INFORMATION

Corresponding Authors

Rubel Chakravarty – Radiopharmaceuticals Division, Bhabha Atomic Research Centre, Trombay, Mumbai 400085, India; Homi Bhabha National Institute, Anushaktinagar, Mumbai 400094, India; orcid.org/0000-0003-2125-8636; Email: rubelc@barc.gov.in, rubelchakravarty@gmail.com

Weibo Cai – Departments of Radiology and Medical Physics, University of Wisconsin-Madison, Madison, Wisconsin 53705, United States; orcid.org/0000-0003-4641-0833; Email: wcai@uwhealth.org

Authors

Sanchita Ghosh – Radiopharmaceuticals Division, Bhabha Atomic Research Centre, Trombay, Mumbai 400085, India; Homi Bhabha National Institute, Anushaktinagar, Mumbai 400094, India

Sophia J. Lee – Departments of Radiology and Medical Physics, University of Wisconsin-Madison, Madison, Wisconsin 53705, United States

Jessica C. Hsu – Departments of Radiology and Medical Physics, University of Wisconsin-Madison, Madison, Wisconsin 53705, United States

Sudipta Chakraborty – Radiopharmaceuticals Division, Bhabha Atomic Research Centre, Trombay, Mumbai 400085, India; Homi Bhabha National Institute, Anushaktinagar, Mumbai 400094, India; orcid.org/0000-0002-8002-439X

Complete contact information is available at: <https://pubs.acs.org/10.1021/cbmi.3c00092>

Notes

The authors declare the following competing financial interest(s): W.C. declares a conflict of interest with the following corporations: Actithera, Inc., Rad Source Technologies, Inc., Portrai, Inc., rTR Technovation Corporation, and Four Health Global Pharmaceuticals Inc.. All other authors declare no conflict of interest.

ACKNOWLEDGMENTS

The authors are grateful for the financial support from the Bhabha Atomic Research Centre, the University of Wisconsin—Madison, and the National Institutes of Health (P30 CA014520 and T32 CA009206).

VOCABULARY

Brachytherapy, It is a cancer treatment modality in which radioactivity sealed inside a seed, pellet, wire, or capsule is implanted inside the patient body using a needle or catheter; **Molecular imaging**, It is the noninvasive visualization, assessment, and measurement of biological processes at the molecular and cellular level in living subjects; **Nanomedicine**, It is a medical specialty that utilizes nanotechnology for diagnosis and treatment of diseases; **Nanoscale brachytherapy**, A minimally invasive therapeutic procedure involving intratumoral injection of functionalized nanoparticles labeled with a therapeutic radioisotope; **Radiation dosimetry**, It refers to the science by which radiation dose is planned by measurement, calculation, or a combination of measurement and calculation, and assigning the doses to individuals; **Radiolabeling of nanoparticles**, Incorporation of a suitable radioisotope in the nanoplateform for imaging and/or therapy; **Theranostics**, It refers to the concept of pairing diagnostic biomarkers with therapeutic agents to share a precise target for personalizing disease intervention

REFERENCES

- (1) Sung, H.; Ferlay, J.; Siegel, R. L.; Laversanne, M.; Soerjomataram, I.; Jemal, A.; Bray, F. Global Cancer Statistics 2020: GLOBOCAN Estimates of Incidence and Mortality Worldwide for 36 Cancers in 185 Countries. *CA Cancer J. Clin* **2021**, *71* (3), 209–249.
- (2) Baskar, R.; Lee, K. A.; Yeo, R.; Yeoh, K. W. Cancer and radiation therapy: current advances and future directions. *Int. J. Med. Sci.* **2012**, *9* (3), 193–9.
- (3) Chaput, G.; Regnier, L. Radiotherapy: Clinical pearls for primary care. *Can. Fam Physician* **2021**, *67* (10), 753–757.
- (4) Wang, J.; Chen, Y.; Xie, H.; Luo, L.; Tang, Q. Evaluation of auto-segmentation for EBRT planning structures using deep learning-based workflow on cervical cancer. *Sci. Rep.* **2022**, *12* (1), 13650.
- (5) Gillings, N.; Hjelstuen, O.; Ballinger, J.; Behe, M.; Decristoforo, C.; Elsinga, P.; Ferrari, V.; Peitl, P. K.; Kozirowski, J.; Laverman, P.; Mindt, T. L.; Neels, O.; Ocak, M.; Patt, M.; Todde, S. Guideline on current good radiopharmacy practice (cGRPP) for the small-scale preparation of radiopharmaceuticals. *EJNMMI Radiopharmacy and Chemistry* **2021**, *6* (1), 8.
- (6) Chakravarty, R.; Chakraborty, S.; Vimalnath, K.; Shetty, P.; Sarma, H. D.; Hassan, P.; Dash, A. $^{64}\text{CuCl}_2$ produced by direct neutron activation route as a cost-effective probe for cancer imaging: the journey has begun. *RSC Adv.* **2015**, *5* (111), 91723–91733.
- (7) Chakravarty, R.; Shetty, P.; Nair, K. V.; Rajeswari, A.; Jagadeesan, K.; Sarma, H. D.; Rangarajan, V.; Krishnatry, R.; Chakraborty, S. Reactor produced ^{64}Cu CuCl_2 as a PET radiopharmaceutical for cancer imaging: From radiochemistry laboratory to nuclear medicine clinic. *Annals of Nuclear Medicine* **2020**, *34*, 899–910.

- (8) Chakravarty, R.; Chakraborty, S.; Dash, A. $^{64}\text{Cu}^{2+}$ ions as PET probe: an emerging paradigm in molecular imaging of cancer. *Mol. Pharmaceutics* **2016**, *13* (11), 3601–3612.
- (9) Chargari, C.; Deutsch, E.; Blanchard, P.; Gouy, S.; Martelli, H.; Guérin, F.; Dumas, I.; Bossi, A.; Morice, P.; Viswanathan, A. N.; Haie-Meder, C. Brachytherapy: An overview for clinicians. *CA Cancer J. Clin* **2019**, *69* (5), 386–401.
- (10) Deng, X.; Wu, H.; Gao, F.; Su, Y.; Li, Q.; Liu, S.; Cai, J. Brachytherapy in the treatment of breast cancer. *Int. J. Clin Oncol* **2017**, *22* (4), 641–650.
- (11) Hannoun-Lévi, J. M.; Chargari, C.; Blanchard, P.; Pommier, P.; Ollivier, L.; Ferré, M.; Peiffert, D. Best practice in brachytherapy. *Cancer Radiother* **2022**, *26* (1–2), 29–33.
- (12) Tanderup, K.; Ménard, C.; Polgar, C.; Lindegaard, J. C.; Kirisits, C.; Pötter, R. Advancements in brachytherapy. *Adv. Drug Deliv Rev.* **2017**, *109*, 15–25.
- (13) Wallner, K.; Delouya, G.; Quang, T. S. Medical malpractice and brachytherapy. *Brachytherapy* **2021**, *20* (5), 950–955.
- (14) Zaorsky, N. G.; Davis, B. J.; Nguyen, P. L.; Showalter, T. N.; Hoskin, P. J.; Yoshioka, Y.; Morton, G. C.; Horwitz, E. M. The evolution of brachytherapy for prostate cancer. *Nat. Rev. Urol* **2017**, *14* (7), 415–439.
- (15) Davis, B. J.; Horwitz, E. M.; Lee, W. R.; Crook, J. M.; Stock, R. G.; Merrick, G. S.; Butler, W. M.; Grimm, P. D.; Stone, N. N.; Potters, L.; Zietman, A. L.; Zelefsky, M. J. American Brachytherapy Society consensus guidelines for transrectal ultrasound-guided permanent prostate brachytherapy. *Brachytherapy* **2012**, *11* (1), 6–19.
- (16) Polgár, C.; Ott, O. J.; Hildebrandt, G.; Kauer-Dorner, D.; Knauerhase, H.; Major, T.; Lyczek, J.; Guinot, J. L.; Dunst, J.; Miguelez, C. G.; Slampa, P.; Allgäuer, M.; Lössl, K.; Polat, B.; Kovács, G.; Fishedick, A. R.; Fietkau, R.; Resch, A.; Kulik, A.; Arribas, L.; Niehoff, P.; Guedea, F.; Schlamann, A.; Pötter, R.; Gall, C.; Uter, W.; Strnad, V. Late side-effects and cosmetic results of accelerated partial breast irradiation with interstitial brachytherapy versus whole-breast irradiation after breast-conserving surgery for low-risk invasive and in-situ carcinoma of the female breast: 5-year results of a randomised, controlled, phase 3 trial. *Lancet Oncol* **2017**, *18* (2), 259–268.
- (17) Ehlerding, E. B.; Cai, W. Smaller Agents for Larger Therapeutic Indices: Nanoscale Brachytherapy with ^{177}Lu -Labeled Gold Nanoparticles. *J. Nucl. Med.* **2016**, *57* (6), 834–5.
- (18) Seniwal, B.; Thiye, V. C.; Singh, S.; Fonseca, T. C. F.; Freitas de Freitas, L. Recent Advances in Brachytherapy Using Radioactive Nanoparticles: An Alternative to Seed-Based Brachytherapy. *Front Oncol* **2021**, *11*, 766407.
- (19) Kono, Y.; Kubota, K.; Mitsumoto, T.; Tanaka, A.; Ishibashi, A.; Kobayashi, K.; Ito, K.; Itami, J.; Kanemura, M.; Minowada, S. Scintigraphic Detection of ^{125}I Seeds After Permanent Brachytherapy for Prostate Cancer. *J. Nucl. Med.* **2008**, *49* (4), 541.
- (20) Hruby, M.; Pouckova, P.; Zadinova, M.; Kucka, J.; Lebeda, O. Thermoresponsive polymeric radionuclide delivery system—an injectable brachytherapy. *Eur. J. Pharm. Sci.* **2011**, *42* (5), 484–8.
- (21) Laprise-Pelletier, M.; Ma, Y.; Lagueux, J.; Côté, M. F.; Beaulieu, L.; Fortin, M. A. Intratumoral Injection of Low-Energy Photon-Emitting Gold Nanoparticles: A Microdosimetric Monte Carlo-Based Model. *ACS Nano* **2018**, *12* (3), 2482–2497.
- (22) Lin, M. Y.; Hsieh, H. H.; Chen, J. C.; Chen, C. L.; Sheu, N. C.; Huang, W. S.; Ho, S. Y.; Chen, T. W.; Lee, Y. J.; Wu, C. Y. Brachytherapy Approach Using ^{177}Lu Conjugated Gold Nanostars and Evaluation of Biodistribution, Tumor Retention, Dosimetry and Therapeutic Efficacy in Head and Neck Tumor Model. *Pharmaceutics* **2021**, *13* (11), 1903.
- (23) Moeendarbari, S.; Tekade, R.; Mulgaonkar, A.; Christensen, P.; Ramezani, S.; Hassan, G.; Jiang, R.; Öz, O. K.; Hao, Y.; Sun, X. Theranostic Nanoseeds for Efficacious Internal Radiation Therapy of Unresectable Solid Tumors. *Sci. Rep* **2016**, *6*, 20614.
- (24) Laprise-Pelletier, M.; Simão, T.; Fortin, M. A. Gold Nanoparticles in Radiotherapy and Recent Progress in Nano-brachytherapy. *Adv. Healthc Mater.* **2018**, *7* (16), No. e1701460.
- (25) Chao, Y.; Liang, C.; Yang, Y.; Wang, G.; Maiti, D.; Tian, L.; Wang, F.; Pan, W.; Wu, S.; Yang, K.; Liu, Z. Highly Effective Radioisotope Cancer Therapy with a Non-Therapeutic Isotope Delivered and Sensitized by Nanoscale Coordination Polymers. *ACS Nano* **2018**, *12* (8), 7519–7528.
- (26) Rahmim, A.; Zaidi, H. PET versus SPECT: strengths, limitations and challenges. *Nuclear medicine communications* **2008**, *29* (3), 193–207.
- (27) Terreno, E.; Castelli, D. D.; Viale, A.; Aime, S. Challenges for molecular magnetic resonance imaging. *Chem. Rev.* **2010**, *110* (5), 3019–3042.
- (28) Liu, Y.; Ai, K.; Lu, L. Nanoparticulate X-ray computed tomography contrast agents: from design validation to in vivo applications. *Accounts of chemical research* **2012**, *45* (10), 1817–1827.
- (29) Peng, Y.; Xiong, B.; Peng, L.; Li, H.; He, Y.; Yeung, E. S. Recent advances in optical imaging with anisotropic plasmonic nanoparticles. *Anal. Chem.* **2015**, *87* (1), 200–215.
- (30) Zhang, G.; Ye, H.-R.; Sun, Y.; Guo, Z.-Z. Ultrasound Molecular Imaging and Its Applications in Cancer Diagnosis and Therapy. *ACS sensors* **2022**, *7* (10), 2857–2864.
- (31) Ni, D.; Jiang, D.; Ehlerding, E. B.; Huang, P.; Cai, W. Radiolabeling Silica-Based Nanoparticles via Coordination Chemistry: Basic Principles, Strategies, and Applications. *Acc. Chem. Res.* **2018**, *51* (3), 778–788.
- (32) Sun, X.; Cai, W.; Chen, X. Positron emission tomography imaging using radiolabeled inorganic nanomaterials. *Acc. Chem. Res.* **2015**, *48* (2), 286–94.
- (33) Coenen, H. H.; Gee, A. D.; Adam, M.; Antoni, G.; Cutler, C. S.; Fujibayashi, Y.; Jeong, J. M.; Mach, R. H.; Mindt, T. L.; Pike, V. W.; Windhorst, A. D. Open letter to journal editors on: International Consensus Radiochemistry Nomenclature Guidelines. *Ann. Nucl. Med.* **2018**, *32* (3), 236–238.
- (34) Meyer, J. P.; Adumeau, P.; Lewis, J. S.; Zeglis, B. M. Click Chemistry and Radiochemistry: The First 10 Years. *Bioconjug Chem.* **2016**, *27* (12), 2791–2807.
- (35) Price, E. W.; Orvig, C. Matching chelators to radiometals for radiopharmaceuticals. *Chem. Soc. Rev.* **2014**, *43* (1), 260–290.
- (36) Wadas, T. J.; Wong, E. H.; Weisman, G. R.; Anderson, C. J. Coordinating radiometals of copper, gallium, indium, yttrium, and zirconium for PET and SPECT imaging of disease. *Chem. Rev.* **2010**, *110* (5), 2858–902.
- (37) Pimlott, S. L.; Sutherland, A. Molecular tracers for the PET and SPECT imaging of disease. *Chem. Soc. Rev.* **2011**, *40* (1), 149–162.
- (38) Hu, A.; Wilson, J. J. Advancing Chelation Strategies for Large Metal Ions for Nuclear Medicine Applications. *Acc. Chem. Res.* **2022**, *55* (6), 904–915.
- (39) Deng, H.; Wang, H.; Li, Z. Matching Chelators to Radiometals for Positron Emission Tomography Imaging-Guided Targeted Drug Delivery. *Curr. Drug Targets* **2015**, *16* (6), 610–24.
- (40) Price, E. W.; Orvig, C. Matching chelators to radiometals for radiopharmaceuticals. *Chem. Soc. Rev.* **2014**, *43* (1), 260–90.
- (41) Price, E. W.; Zeglis, B. M.; Cawthray, J. F.; Lewis, J. S.; Adam, M. J.; Orvig, C. What a difference a carbon makes: $\text{H}_4\text{C}_8\text{octa}$ vs $\text{H}_4\text{C}_3\text{octa}$, ligands for In-111 and Lu-177 radiochemistry. *Inorg. Chem.* **2014**, *53* (19), 10412–31.
- (42) Tei, L.; Baranyai, Z.; Brücher, E.; Cassino, C.; Demicheli, F.; Masciocchi, N.; Giovenzana, G. B.; Botta, M. Dramatic Increase of Selectivity for Heavy Lanthanide(III) Cations by Tuning the Flexibility of Polydentate Chelators. *Inorg. Chem.* **2010**, *49* (2), 616–625.
- (43) Kozirowski, J.; Stanciu, A. E.; Gomez-Vallejo, V.; Llop, J. Radiolabeled nanoparticles for cancer diagnosis and therapy. *Anti-Cancer Agents in Medicinal Chemistry (Formerly Current Medicinal Chemistry-Anti-Cancer Agents)* **2017**, *17* (3), 333–354.
- (44) Ambrogio, M. W.; Toro-González, M.; Keever, T. J.; McKnight, T. E.; Davern, S. M. Poly(lactic-co-glycolic acid) Nanoparticles as Delivery Systems for the Improved Administration of Radiotherapeutic Anticancer Agents. *ACS Applied Nano Materials* **2020**, *3* (11), 10565–10570.

- (45) Martínez Martínez, T.; García Aliaga, A.; López-González, I.; Abella Tarazona, A.; Ibáñez Ibáñez, M. J.; Cenis, J. L.; Meseguer-Olmo, L.; Lozano-Pérez, A. A. Fluorescent DTPA-Silk Fibroin Nanoparticles Radiolabeled with ^{111}In : A Dual Tool for Biodistribution and Stability Studies. *ACS Biomaterials Science & Engineering* **2020**, *6* (6), 3299–3309.
- (46) de Barros, A. B.; Tsourkas, A.; Saboury, B.; Cardoso, V. N.; Alavi, A. Emerging role of radiolabeled nanoparticles as an effective diagnostic technique. *EJNMMI Research* **2012**, *2* (1), 39.
- (47) Pérez-Campaña, C.; Gómez-Vallejo, V.; Martín, A.; San Sebastián, E.; Moya, S. E.; Reese, T.; Ziolo, R. F.; Llop, J. Tracing nanoparticles in vivo: a new general synthesis of positron emitting metal oxide nanoparticles by proton beam activation. *Analyst* **2012**, *137* (21), 4902–6.
- (48) Pérez-Campaña, C.; Gómez-Vallejo, V.; Puigvila, M.; Martín, A.; Calvo-Fernández, T.; Moya, S. E.; Ziolo, R. F.; Reese, T.; Llop, J. Biodistribution of different sized nanoparticles assessed by positron emission tomography: a general strategy for direct activation of metal oxide particles. *ACS Nano* **2013**, *7* (4), 3498–505.
- (49) Di Pasqua, A. J.; Yuan, H.; Chung, Y.; Kim, J. K.; Huckle, J. E.; Li, C.; Sadgrove, M.; Tran, T. H.; Jay, M.; Lu, X. Neutron-activatable holmium-containing mesoporous silica nanoparticles as a potential radionuclide therapeutic agent for ovarian cancer. *J. Nucl. Med.* **2013**, *54* (1), 111–6.
- (50) da Silva, W. M.; de Andrade Alves, E. S. R. H.; Cipreste, M. F.; Andrade, G. F.; Gastelois, P. L.; de Almeida Macedo, W. A.; de Sousa, E. M. B. Boron nitride nanotubes radiolabeled with ^{153}Sm and ^{159}Gd : Potential application in nanomedicine. *Appl. Radiat. Isot.* **2020**, *157*, 109032.
- (51) Chen, Z.; Yang, Q.; Song, L.; Qiu, Y.; Wu, S.; Huang, W.; Jiang, Q.; Wu, S.; Kang, L. A novel tetrapeptide for chelator-free radiolabeling in optimized preparation of $^{99\text{m}}\text{Tc}$ -radiolabeled oligonucleotides. *Am. J. Nucl. Med. Mol. Imaging* **2022**, *12* (5), 143–151.
- (52) Papadopoulou, S.; Kolokithas-Ntoukas, A.; Salvanou, E. A.; Gaitanis, A.; Xanthopoulos, S.; Avgoustakis, K.; Gazouli, M.; Paravatou-Petsotas, M.; Tsoukalas, C.; Bakandritsos, A.; Bouziotis, P. Chelator-Free/Chelator-Mediated Radiolabeling of Colloidally Stabilized Iron Oxide Nanoparticles for Biomedical Imaging. *Nanomaterials (Basel)* **2021**, *11* (7), 1677.
- (53) Patra, S.; Kancharlapalli, S.; Chakraborty, A.; Singh, K.; Kumar, C.; Guleria, A.; Rakshit, S.; Damle, A.; Chakravarty, R.; Chakraborty, S. Chelator-Free Radiolabeling with Theoretical Insights and Preclinical Evaluation of Citrate-Functionalized Hydroxyapatite Nanospheres for Potential Use as Radionanomedicine. *Ind. Eng. Chem. Res.* **2023**, *62* (7), 3194–3205.
- (54) Chen, F.; Ellison, P. A.; Lewis, C. M.; Hong, H.; Zhang, Y.; Shi, S.; Hernandez, R.; Meyerand, M. E.; Barnhart, T. E.; Cai, W. Chelator-free synthesis of a dual-modality PET/MRI agent. *Angew. Chem., Int. Ed. Engl.* **2013**, *52* (50), 13319–23.
- (55) Belderbos, S.; González-Gómez, M. A.; Cleeren, F.; Wouters, J.; Piñeiro, Y.; Deroose, C. M.; Coosemans, A.; Gsell, W.; Borrmans, G.; Rivas, J.; Himmelreich, U. Simultaneous in vivo PET/MRI using fluorine-18 labeled $\text{Fe}_3\text{O}_4@Al(\text{OH})_3$ nanoparticles: comparison of nanoparticle and nanoparticle-labeled stem cell distribution. *EJNMMI Res.* **2020**, *10* (1), 73.
- (56) Liu, Q.; Sun, Y.; Li, C.; Zhou, J.; Li, C.; Yang, T.; Zhang, X.; Yi, T.; Wu, D.; Li, F. ^{18}F -Labeled magnetic-upconversion nanophosphors via rare-Earth cation-assisted ligand assembly. *ACS Nano* **2011**, *5* (4), 3146–57.
- (57) Chakravarty, R.; Chakraborty, S.; Guleria, A.; Kumar, C.; Kunwar, A.; Nair, K. V. V.; Sarma, H. D.; Dash, A. Clinical scale synthesis of intrinsically radiolabeled and cyclic RGD peptide functionalized ^{198}Au nanoparticles for targeted cancer therapy. *Nuclear Medicine and Biology* **2019**, *72–73*, 1–10.
- (58) Kjekorjian, M.; Sandker, G. G. W.; Cortenbach, K. R. G.; Tagit, O.; van Riessen, N. K.; Raavé, R.; Srinivas, M.; Figdor, C. G.; Heskamp, S.; Aarntzen, E. Characterization of Intrinsically Radiolabeled Poly(lactic-co-glycolic acid) Nanoparticles for ex Vivo Autologous Cell Labeling and in Vivo Tracking. *Bioconj. Chem.* **2021**, *32* (8), 1802–1811.
- (59) Chakravarty, R.; Chakraborty, S.; Guleria, A.; Kumar, C.; Kunwar, A.; Nair, K. V. V.; Sarma, H. D.; Dash, A. Clinical scale synthesis of intrinsically radiolabeled and cyclic RGD peptide functionalized ^{198}Au nanoparticles for targeted cancer therapy. *Nucl. Med. Biol.* **2019**, *72–73*, 1–10.
- (60) Chakravarty, R.; Chakraborty, S.; Guleria, A.; Shukla, R.; Kumar, C.; Vimalnath Nair, K. V.; Sarma, H. D.; Tyagi, A. K.; Dash, A. Facile One-Pot Synthesis of Intrinsically Radiolabeled and Cyclic RGD Conjugated ^{199}Au Nanoparticles for Potential Use in Nanoscale Brachytherapy. *Ind. Eng. Chem. Res.* **2018**, *57* (43), 14337–14346.
- (61) Chakravarty, R.; Chakraborty, S.; Ningthoujam, R. S.; Vimalnath Nair, K. V.; Sharma, K. S.; Ballal, A.; Guleria, A.; Kunwar, A.; Sarma, H. D.; Vatsa, R. K.; Dash, A. Industrial-Scale Synthesis of Intrinsically Radiolabeled ^{64}CuS Nanoparticles for Use in Positron Emission Tomography (PET) Imaging of Cancer. *Ind. Eng. Chem. Res.* **2016**, *55* (48), 12407–12419.
- (62) Kreyling, W. G.; Möller, W.; Holzwarth, U.; Hirn, S.; Wenk, A.; Schleh, C.; Schäffler, M.; Haberl, N.; Gibson, N.; Schittny, J. C. Age-Dependent Rat Lung Deposition Patterns of Inhaled 20 Nanometer Gold Nanoparticles and their Quantitative Biokinetics in Adult Rats. *ACS Nano* **2018**, *12* (8), 7771–7790.
- (63) Wang, Y.; Liu, Y.; Luehmann, H.; Xia, X.; Wan, D.; Cutler, C.; Xia, Y. Radioluminescent gold nanocages with controlled radioactivity for real-time in vivo imaging. *Nano Lett.* **2013**, *13* (2), 581–5.
- (64) Pouliquen, D.; Perdrisot, R.; Ermias, A.; Akoka, S.; Jallet, P.; Le Jeune, J. J. Superparamagnetic iron oxide nanoparticles as a liver MRI contrast agent: contribution of microencapsulation to improved biodistribution. *Magn Reson Imaging* **1989**, *7* (6), 619–27.
- (65) Poty, S.; Francesconi, L. C.; McDevitt, M. R.; Morris, M. J.; Lewis, J. S. α -Emitters for Radiotherapy: From Basic Radiochemistry to Clinical Studies-Part I. *J. Nucl. Med.* **2018**, *59* (6), 878–884.
- (66) Mulford, D. A.; Scheinberg, D. A.; Jurcic, J. G. The promise of targeted α -particle therapy. *J. Nucl. Med.* **2005**, *46* (1 suppl), 199S–204S.
- (67) Feuerecker, B.; Kratochwil, C.; Ahmadzadehfar, H.; Morgenstern, A.; Eiber, M.; Herrmann, K.; Pomykala, K. L. Clinical Translation of Targeted α -Therapy: An Evolution or a Revolution? *J. Nucl. Med.* **2023**, *64* (5), 685–692.
- (68) Shah, H. J.; Ruppell, E.; Bokhari, R.; Aland, P.; Lele, V. R.; Ge, C.; McIntosh, L. J. Current and upcoming radionuclide therapies in the direction of precision oncology: A narrative review. *Eur. J. Radiol. Open* **2023**, *10*, 100477.
- (69) Guérard, F.; Maingueneau, C.; Liu, L.; Eychenne, R.; Gustin, J.-F.; Montavon, G.; Galland, N. Advances in the Chemistry of Astatine and Implications for the Development of Radiopharmaceuticals. *Acc. Chem. Res.* **2021**, *54* (16), 3264–3275.
- (70) Aghevlian, S.; Boyle, A. J.; Reilly, R. M. Radioimmunotherapy of cancer with high linear energy transfer (LET) radiation delivered by radionuclides emitting α -particles or Auger electrons. *Adv. Drug Deliv. Rev.* **2017**, *109*, 102–118.
- (71) Ku, A.; Facca, V. J.; Cai, Z.; Reilly, R. M. Auger electrons for cancer therapy - a review. *EJNMMI Radiopharm. Chem.* **2019**, *4* (1), 27.
- (72) Buchegger, F.; Perillo-Adamer, F.; Dupertuis, Y. M.; Bischof Delaloye, A. Auger radiation targeted into DNA: a therapy perspective. *Eur. J. Nucl. Med. Mol. Imaging* **2006**, *33* (11), 1352–63.
- (73) Lee, L. J.; Das, I. J.; Higgins, S. A.; Jhingran, A.; Small, W.; Thomadsen, B.; Viswanathan, A. N.; Wolfson, A.; Eifel, P. American Brachytherapy Society consensus guidelines for locally advanced carcinoma of the cervix. Part III: Low-dose-rate and pulsed-dose-rate brachytherapy. *Brachytherapy* **2012**, *11* (1), 53–57.
- (74) Mancini-Terracciano, C.; Donnarumma, R.; Bencivenga, G.; Bocci, V.; Cartoni, A.; Collamati, F.; Fratoddi, I.; Giordano, A.; Indovina, L.; Maccora, D.; Marafini, M.; Mirabelli, R.; Morganti, S.; Rotili, D.; Russomando, A.; Scotognella, T.; Solfaroli Camillocci, E.; Toppi, M.; Traini, G.; Venditti, I.; Faccini, R. Feasibility of beta-

particle radioguided surgery for a variety of "nuclear medicine" radionuclides. *Phys. Med.* **2017**, *43*, 127–133.

(75) Zoller, F.; Eisenhut, M.; Haberkorn, U.; Mier, W. Endoradiotherapy in cancer treatment-basic concepts and future trends. *Eur. J. Pharmacol.* **2009**, *625* (1–3), 55–62.

(76) Meredith, R. F.; Torgue, J. J.; Rozgaja, T. A.; Banaga, E. P.; Bunch, P. W.; Alvarez, R. D.; Straughn, J. M., Jr.; Dobelbower, M. C.; Lowy, A. M. Safety and Outcome Measures of First-in-Human Intraperitoneal α Radioimmunotherapy With 212Pb-TCMC-Trastuzumab. *Am. J. Clin. Oncol.* **2018**, *41* (7), 716–721.

(77) Cai, Z.; Chattopadhyay, N.; Yang, K.; Kwon, Y. L.; Yook, S.; Pignol, J. P.; Reilly, R. M. ¹¹¹In-labeled trastuzumab-modified gold nanoparticles are cytotoxic in vitro to HER2-positive breast cancer cells and arrest tumor growth in vivo in athymic mice after intratumoral injection. *Nucl. Med. Biol.* **2016**, *43* (12), 818–826.

(78) Chakravarty, R.; Chakraborty, S. A review of advances in the last decade on targeted cancer therapy using (177)Lu: focusing on ¹⁷⁷Lu produced by the direct neutron activation route. *Am. J. Nucl. Med. Mol. Imaging* **2021**, *11* (6), 443–475.

(79) Czerwińska, M.; Bilewicz, A.; Kruszewski, M.; Wegierek-Ciuk, A.; Lankoff, A. Targeted Radionuclide Therapy of Prostate Cancer-From Basic Research to Clinical Perspectives. *Molecules* **2020**, *25* (7), 1743.

(80) Donahue, N. D.; Acar, H.; Wilhelm, S. Concepts of nanoparticle cellular uptake, intracellular trafficking, and kinetics in nanomedicine. *Adv. Drug Deliv. Rev.* **2019**, *143*, 68–96.

(81) Kaksonen, M.; Roux, A. Mechanisms of clathrin-mediated endocytosis. *Nat. Rev. Mol. Cell Biol.* **2018**, *19* (5), 313–326.

(82) Conner, S. D.; Schmid, S. L. Regulated portals of entry into the cell. *Nature* **2003**, *422* (6927), 37–44.

(83) Foerg, C.; Ziegler, U.; Fernandez-Carneado, J.; Giralt, E.; Rennert, R.; Beck-Sickinger, A. G.; Merkle, H. P. Decoding the entry of two novel cell-penetrating peptides in HeLa cells: lipid raft-mediated endocytosis and endosomal escape. *Biochemistry* **2005**, *44* (1), 72–81.

(84) Chen, X.; Shank, S.; Davis, P. B.; Ziady, A. G. Nucleolin-mediated cellular trafficking of DNA nanoparticle is lipid raft and microtubule dependent and can be modulated by glucocorticoid. *Mol. Ther.* **2011**, *19* (1), 93–102.

(85) Sosale, N. G.; Ivanovska, I. I.; Tsai, R. K.; Swift, J.; Hsu, J. W.; Alvey, C. M.; Zoltick, P. W.; Discher, D. E. "Marker of Self" CD47 on lentiviral vectors decreases macrophage-mediated clearance and increases delivery to SIRPA-expressing lung carcinoma tumors. *Mol. Ther. Methods Clin. Dev.* **2016**, *3*, 16080.

(86) Kerr, M. C.; Teasdale, R. D. Defining macropinocytosis. *Traffic* **2009**, *10* (4), 364–71.

(87) Gentile, F.; Chiappini, C.; Fine, D.; Bhavane, R. C.; Peluccio, M. S.; Cheng, M. M.; Liu, X.; Ferrari, M.; Decuzzi, P. The effect of shape on the margination dynamics of non-neutrally buoyant particles in two-dimensional shear flows. *J. Biomech.* **2008**, *41* (10), 2312–8.

(88) Thurston, G.; McLean, J. W.; Rizen, M.; Baluk, P.; Haskell, A.; Murphy, T. J.; Hanahan, D.; McDonald, D. M. Cationic liposomes target angiogenic endothelial cells in tumors and chronic inflammation in mice. *J. Clin. Invest.* **1998**, *101* (7), 1401–13.

(89) Hao, X.; Wu, J.; Shan, Y.; Cai, M.; Shang, X.; Jiang, J.; Wang, H. Caveolae-mediated endocytosis of biocompatible gold nanoparticles in living HeLa cells. *J. Phys.: Condens. Matter* **2012**, *24* (16), 164207.

(90) Ng, C. T.; Tang, F. M.; Li, J. J.; Ong, C.; Yung, L. L.; Bay, B. H. Clathrin-mediated endocytosis of gold nanoparticles in vitro. *Anat. Rec. (Hoboken)* **2015**, *298* (2), 418–27.

(91) Bannunah, A. M.; Vllasaliu, D.; Lord, J.; Stolnik, S. Mechanisms of nanoparticle internalization and transport across an intestinal epithelial cell model: effect of size and surface charge. *Mol. Pharmaceutics* **2014**, *11* (12), 4363–73.

(92) Chakravarty, R.; Lan, X.; Chakraborty, S.; Cai, W. Astatine-211 for PSMA-targeted α -radiation therapy of micrometastatic prostate cancer: a sustainable approach towards precision oncology. *Eur. J. Nucl. Med. Mol. Imaging* **2023**, *50* (7), 1844–1847.

(93) Dziawer, Ł.; Majkowska-Pilip, A.; Gawel, D.; Godlewska, M.; Pruszyński, M.; Jastrzębski, J.; Wąs, B.; Bilewicz, A. Trastuzumab-Modified Gold Nanoparticles Labeled with ²¹¹At as a Prospective Tool for Local Treatment of HER2-Positive Breast Cancer. *Nanomaterials (Basel)* **2019**, *9* (4), 632.

(94) Salvanou, E. A.; Stellas, D.; Tsoukalas, C.; Mavroidi, B.; Paravatou-Petsotas, M.; Kalogeropoulos, N.; Xanthopoulos, S.; Denat, F.; Laurent, G.; Bazzi, R.; Roux, S.; Bouziotis, P. A Proof-of-Concept Study on the Therapeutic Potential of Au Nanoparticles Radiolabeled with the Alpha-Emitter Actinium-225. *Pharmaceutics* **2020**, *12* (2), 188.

(95) Kato, H.; Huang, X.; Kadonaga, Y.; Katayama, D.; Ooe, K.; Shimoyama, A.; Kabayama, K.; Toyoshima, A.; Shinohara, A.; Hatazawa, J.; Fukase, K. Intratumoral administration of astatine-211-labeled gold nanoparticle for alpha therapy. *J. Nanobiotechnology* **2021**, *19* (1), 223.

(96) Laprise-Pelletier, M.; Lagueux, J.; Côté, M. F.; LaGrange, T.; Fortin, M. A. Low-Dose Prostate Cancer Brachytherapy with Radioactive Palladium-Gold Nanoparticles. *Adv. Healthc. Mater.* **2017**, *6* (4), 1601120.

(97) Fach, M.; Fliedner, F. P.; Kempen, P. J.; Melander, F.; Hansen, A. E.; Bruun, L. M.; Köster, U.; Sporer, E.; Kjar, A.; Andresen, T. L.; Jensen, A. I.; Henriksen, J. R. Effective Intratumoral Retention of [103Pd]AuPd Alloy Nanoparticles Embedded in Gel-Forming Liquids Paves the Way for New Nanobrachytherapy. *Adv. Healthcare Mater.* **2021**, *10* (10), 2002009.

(98) Zhang, Y.; Sheng, J.; Zhai, F.; Wang, X.; Chen, L.; Shi, C.; Chen, L.; He, L.; Bai, R.; Xie, J.; Chai, Z.; Diwu, J. Pioneering Iodine-125-Labeled Nanoscale Covalent Organic Frameworks for Brachytherapy. *Bioconjug. Chem.* **2021**, *32* (4), 755–762.

(99) Sakr, T. M.; Khowessah, O. M.; Motaleb, M. A.; Abd El-Bary, A.; El-Kolaly, M. T.; Swidan, M. M. I-131 doping of silver nanoparticles platform for tumor theranosis guided drug delivery. *Eur. J. Pharm. Sci.* **2018**, *122*, 239–245.

(100) Stanković, A.; Mihailović, J.; Mirković, M.; Radović, M.; Milanović, Z.; Ognjanović, M.; Janković, D.; Antić, B.; Mijović, M.; Vranješ-Đurić, S.; Prijović, Z. Aminosilanized flower-structured superparamagnetic iron oxide nanoparticles coupled to ¹³¹I-labeled CCP49 antibody for combined radionuclide and hyperthermia therapy of cancer. *Int. J. Pharm.* **2020**, *587*, 119628.

(101) Kelly, G.; Milligan, J. J.; Mastria, E. M.; Kim, S.; Zelenetz, S. R.; Dobbins, J.; Cai, L. Y.; Li, X.; Nair, S. K.; Chilkoti, A. Intratumoral delivery of brachytherapy and immunotherapy by a thermally triggered polypeptide depot. *J. Controlled Release* **2022**, *343*, 267–276.

(102) Sheng, J.; Wang, X.; Yan, J.; Pan, D.; Yang, R.; Wang, L.; Xu, Y.; Yang, M. Theranostic radioiodine-labelled melanin nanoparticles inspired by clinical brachytherapy seeds. *J. Mater. Chem. B* **2018**, *6* (48), 8163–8169.

(103) Viana, R. d. S.; Costa, L. A. d. M.; Harmon, A. C.; Gomes Filho, M. A.; Falcão, E. H. L.; Vicente, M. G. H.; Junior, S. A.; Mathis, J. M. ¹⁷⁷Lu-Labeled Eu-Doped Mesoporous SiO₂ Nanoparticles as a Theranostic Radiopharmaceutical for Colorectal Cancer. *ACS Applied Nano Materials* **2020**, *3* (9), 8691–8701.

(104) Yook, S.; Cai, Z.; Lu, Y.; Winnik, M. A.; Pignol, J. P.; Reilly, R. M. Intratumorally Injected ¹⁷⁷Lu-Labeled Gold Nanoparticles: Gold Nanoseed Brachytherapy with Application for Neoadjuvant Treatment of Locally Advanced Breast Cancer. *J. Nucl. Med.* **2016**, *57* (6), 936–42.

(105) Karpov, T.; Postovalova, A.; Akhmetova, D.; Muslimov, A. R.; Eletskaia, E.; Zyuzin, M. V.; Timin, A. S. Universal Chelator-Free Radiolabeling of Organic and Inorganic-Based Nanocarriers with Diagnostic and Therapeutic Isotopes for Internal Radiotherapy. *Chem. Mater.* **2022**, *34* (14), 6593–6605.

(106) Khan, M. K.; Minc, L. D.; Nigavekar, S. S.; Kariapper, M. S.; Nair, B. M.; Schipper, M.; Cook, A. C.; Lesniak, W. G.; Balogh, L. P. Fabrication of {¹⁹⁸Au⁰} radioactive composite nanodevices and their use for nanobrachytherapy. *Nanomedicine* **2008**, *4* (1), 57–69.

(107) Chanda, N.; Kan, P.; Watkinson, L. D.; Shukla, R.; Zambre, A.; Carmack, T. L.; Engelbrecht, H.; Lever, J. R.; Katti, K.; Fent, G.

M.; Casteel, S. W.; Smith, C. J.; Miller, W. H.; Jurisson, S.; Boote, E.; Robertson, J. D.; Cutler, C.; Dobrovolskaia, M.; Kannan, R.; Katti, K. V. Radioactive gold nanoparticles in cancer therapy: therapeutic efficacy studies of GA-¹⁹⁸AuNP nanoconstruct in prostate tumor-bearing mice. *Nanomedicine* **2010**, *6* (2), 201–9.

(108) Shukla, R.; Chanda, N.; Zambre, A.; Upendran, A.; Katti, K.; Kulkarni, R. R.; Nune, S. K.; Casteel, S. W.; Smith, C. J.; Vimal, J.; Boote, E.; Robertson, J. D.; Kan, P.; Engelbrecht, H.; Watkinson, L. D.; Carmack, T. L.; Lever, J. R.; Cutler, C. S.; Caldwell, C.; Kannan, R.; Katti, K. V. Laminin receptor specific therapeutic gold nanoparticles (¹⁹⁸AuNP-EGCg) show efficacy in treating prostate cancer. *Proc. Natl. Acad. Sci. U. S. A.* **2012**, *109* (31), 12426–31.

(109) Al-Yasiri, A. Y.; Khoobchandani, M.; Cutler, C. S.; Watkinson, L.; Carmack, T.; Smith, C. J.; Kuchuk, M.; Loyalka, S. K.; Lugão, A. B.; Katti, K. V. Mangiferin functionalized radioactive gold nanoparticles (MGF-¹⁹⁸AuNPs) in prostate tumor therapy: green nanotechnology for production, in vivo tumor retention and evaluation of therapeutic efficacy. *Dalton Trans* **2017**, *46* (42), 14561–14571.

(110) Sano, K.; Kanada, Y.; Kanazaki, K.; Ding, N.; Ono, M.; Saji, H. Brachytherapy with Intratumoral Injections of Radiometal-Labeled Polymers That Thermoresponsively Self-Aggregate in Tumor Tissues. *J. Nucl. Med.* **2017**, *58* (9), 1380–1385.

(111) Vukadinović, A.; Milanović, Z.; Ognjanović, M.; Janković, D.; Radović, M.; Mirković, M.; Karageorgou, M. A.; Bouziotis, P.; Erić, S.; Vranješ-Durić, S.; Antić, B.; Prijović, Ž. ⁹⁰Y-CA/SPIONs for dual magnetic hyperthermia-radionuclide nanobrachytherapy of solid tumours. *Nanotechnology* **2022**, *33* (40), 405102.

(112) Fach, M.; Fliedner, F. P.; Kempen, P. J.; Melander, F.; Hansen, A. E.; Bruun, L. M.; Köster, U.; Sporer, E.; Kjaer, A.; Andresen, T. L.; Jensen, A. I.; Henriksen, J. R. Effective Intratumoral Retention of [¹⁰³Pd]AuPd Alloy Nanoparticles Embedded in Gel-Forming Liquids Paves the Way for New Nanobrachytherapy. *Adv. Healthc. Mater.* **2021**, *10* (10), No. e2002009.

(113) Tian, L.; Chen, Q.; Yi, X.; Wang, G.; Chen, J.; Ning, P.; Yang, K.; Liu, Z. Radionuclide I-131 Labeled Albumin-Paclitaxel Nanoparticles for Synergistic Combined Chemo-radioisotope Therapy of Cancer. *Theranostics* **2017**, *7* (3), 614–623.

(114) Ming, H.; Fang, L.; Gao, J.; Li, C.; Ji, Y.; Shen, Y.; Hu, Y.; Li, N.; Chang, J.; Li, W.; Tan, J. Antitumor Effect of Nanoparticle ¹³¹I-Labeled Arginine-Glycine-Aspartate-Bovine Serum Albumin-Polycaprolactone in Lung Cancer. *AJR Am. J. Roentgenol* **2017**, *208* (5), 1116–1126.

(115) Axiak-Bechtel, S. M.; Upendran, A.; Lattimer, J. C.; Kelsey, J.; Cutler, C. S.; Selting, K. A.; Bryan, J. N.; Henry, C. J.; Boote, E.; Tate, D. J.; Bryan, M. E.; Katti, K. V.; Kannan, R. Gum arabic-coated radioactive gold nanoparticles cause no short-term local or systemic toxicity in the clinically relevant canine model of prostate cancer. *Int. J. Nanomedicine* **2014**, *9*, 5001–11.

(116) Fisher, D. R. Internal dosimetry for systemic radiation therapy. *Semin Radiat Oncol* **2000**, *10* (2), 123–32.

(117) Al-Yasiri, A. Y.; White, N. E.; Katti, K. V.; Loyalka, S. K. Estimation of tumor and local tissue dose in gold nanoparticles radiotherapy for prostate cancer. *Rep. Pract. Oncol. Radiother* **2019**, *24* (3), 288–293.

(118) Seniwai, B.; Freitas, L. F.; Mendes, B. M.; Lugão, A. B.; Katti, K. V.; Fonseca, T. C. F. In silico dosimetry of low-dose rate brachytherapy using radioactive nanoparticles. *Phys. Med. Biol.* **2021**, *66* (4), 045016.

(119) Kleynhans, J.; Sathekge, M.; Ebenhan, T. Obstacles and Recommendations for Clinical Translation of Nanoparticle System-Based Targeted Alpha-Particle Therapy. *Materials (Basel)* **2021**, *14* (17), 4784.